et al., 1996; Okada et al., 1998). In addition, Runx1-deficient embryos exhibit defects in vascular branching and remodeling, due to poor release of angiopoietin-1 from hematopoietic stem cells (HSCs) (Takakura et al., 2000). On the other hand, Runx1 has also been implicated in the development of human leukemia. Runx1 is a target of a number of leukemia-associated chromosomal translocations, such as t(8;21)(q22;q22), t(3;21)(q26;q22), and t(12;21)(p12;q22), which generate Runx1/ETO, Runx1/Evi1, and TEL/Runx1 fusion proteins, respectively (Mikhail et al., 2006). In addition, point, deletion, and insertion mutations of Runx1 have also been observed in a significant fraction of acute leukemias (Osato, 2004). Furthermore, a haploinsufficiency of Runx1 was detected in a hereditary familiar platelet disorder in which patients are predisposed to leukemic development (Song et al., 1999). These results demonstrate that structural and functional changes of Runx1 contribute to leukemogenesis.

The expression of Runx1 is controlled by several different mechanisms. Transcription of Runx1 is mediated by two distinct promoters, designated as distal promoter (P1) and proximal promoter (P2), which are located upstream of exon 1 and exon 3, respectively (Ghozi et al., 1996) (see Fig. 1A). Although both promoters are transcriptionally active in both hematopoietic and non-hematopoietic

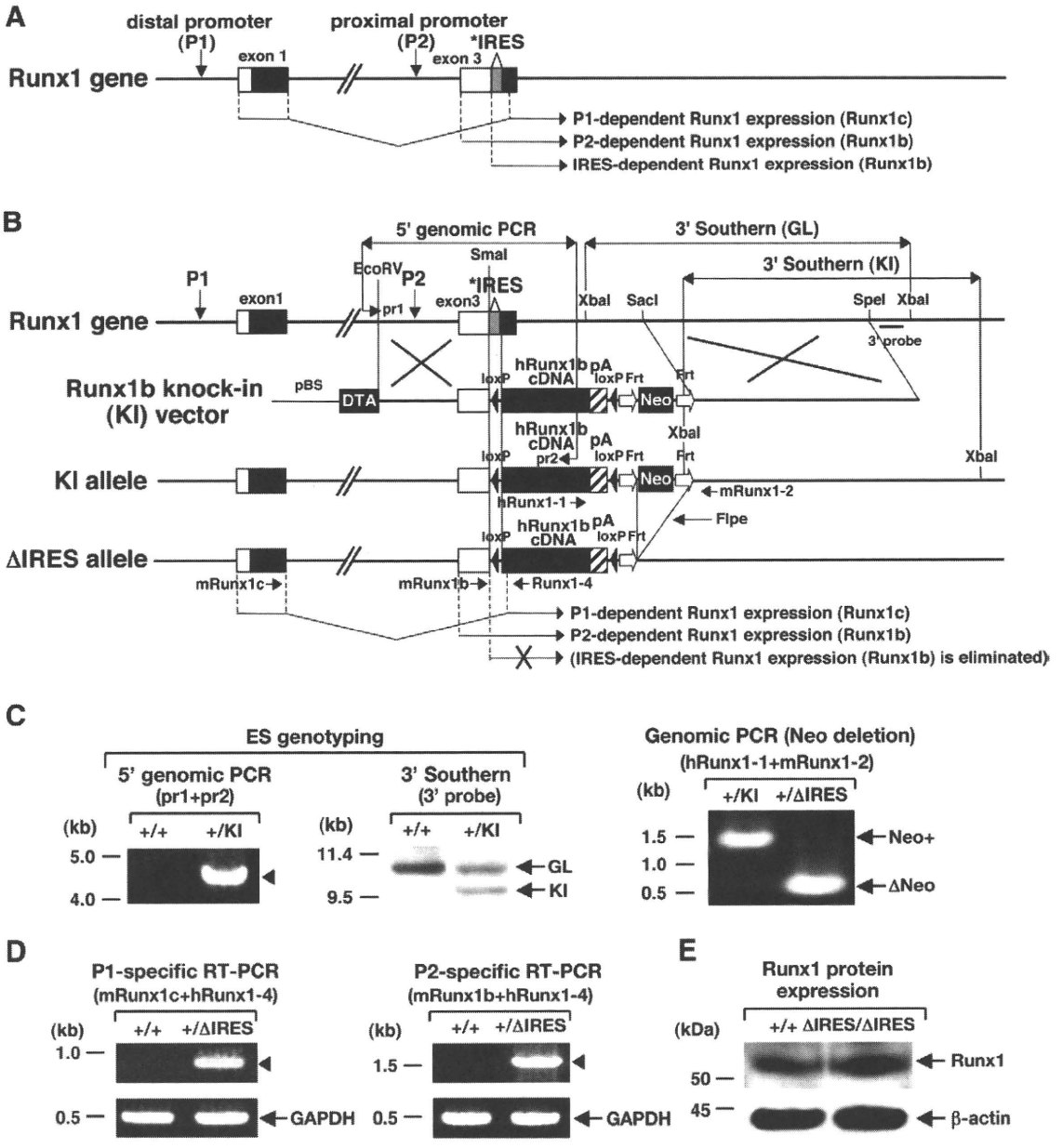

Fig. 1. Genomic organization of the Runx1 gene and generation of Runx1b knock-in (KI) mice deleted with the IRES element (Runx1$^{+/\Delta IRES}$). (A) Regulatory elements controlling Runx1 expression and the resulting gene products. The localizations of exons 1 and 3 and the positions of the distal (P1) and proximal (P2) promoters and the IRES element are shown. The non-coding and coding regions of the exons are indicated by white and black boxes, respectively, and the IRES within the 5′ UTR of exon 3 is indicated by a gray box with an asterisk. The P1-, P2-, and IRES-mediated Runx1 gene products are shown. (B) Strategy for generating Runx1$^{+/\Delta IRES}$ mice. The positions of primers and a probe for genotyping and detecting mRNA expression are shown. In the Runx1$^{+/\Delta IRES}$ mice, expression of both the Runx1c and Runx1b transcripts is retained, but IRES-mediated translation of the Runx1b transcript is eliminated. (C) Results of ES genotyping (left and middle panels) and removal of Neo resistance cassette (right panel). For ES genotyping, the KI allele-derived PCR product is indicated by an arrowhead, and germline (GL) and KI allele-derived DNA fragments are indicated by arrows. For Neo deletion, positions of Neo-positive (Neo+) and Neo-deleted (ΔNeo) PCR products are indicated by arrows. (D) Expression of P1 and P2-derived messages from the ΔIRES allele. The RT-PCR products are indicated by arrowheads (upper panels) and GAPDH RT-PCR was performed as an internal control (lower panels). (E) Expression of Runx1 protein. Nuclear extracts of Runx1$^{+/+}$ and Runx1$^{\Delta IRES/\Delta IRES}$ embryos at 13.5 dpc were blotted with an anti-Runx1 (upper panel) or an anti-β-actin antibody (lower panel).

cells, the structures of the 5′ UTRs of exon 1 and exon 3 are highly diverse (Ghozi et al., 1996). The distal UTR is short, contains only two upstream ATGs (u-ATGs), and lacks GC-rich elements, whereas the proximal UTR is unusually long, contains multiple u-ATGs, and possesses GC-rich regions (Ghozi et al., 1996). These results strongly suggest that the P2-derived message is much poorly transcribed as compared to the P1-derived one. A subsequent study revealed that an IRES element exists in the proximal UTR, just upstream of the translation initiation ATG in exon 3 (see Fig. 1A), whose activity is regulated during differentiation of hematopoietic cells (Pozner et al., 2000; Levanon and Groner, 2004). Taken together, the expression of Runx1 is regulated transcriptionally by two promoters, P1 and P2, and also translationally by an IRES coupled with P2.

Recently, studies using P1-specific knockout ($P1^{N/N}$) mice and P2-specific knockdown ($P2^{neo/neo}$) mice demonstrated that P1-dependent Runx1 expression is not required for embryonic survival but affected hematopoietic development and that P2-dependent Runx1 expression is critical for definitive hematopoiesis, thymic development, and postnatal survival (Pozner et al., 2007; Bee et al., 2010). Although these findings provide insights into the biological roles of the distinct expression machineries of the Runx1 gene, the biological significance of the IRES-mediated translation has not been fully understood.

In this study, to clarify the role of the IRES in Runx1 function under physiological and pathological conditions, we generated and analyzed knock-in mice expressing wild-type Runx1 or a Runx1 fusion protein, in which the 5′ UTR containing the IRES element is deleted.

Materials and methods

Construction of knock-in vectors and generation of knock-in mice

The detailed procedures of construction of knock-in vectors and generation of knock-in mice are described in Supplemental information.

Histological, immunohistochemical, and electron microscopic analyses

Histological, immunohistochemical, and electron microscopic analyses were performed as previously described (Honda et al., 1998). For histological analysis, serial sections (500–1000 slices per embryo) were made and carefully observed under a microscope. For immunohistochemical analysis, tissue sections were stained with an anti-Runx1 antibody (ab61753, Abcam Inc. Cambridge, MA) or an anti-SMA antibody (1A4, Dako, Glostrup, Denmark). For electron microscopic analysis, subcutaneous vessels were subjected to ultra-thin sectioning and examined under an electron microscope after double staining with uranyl acetate and lead citrate.

Reverse transcription polymerase chain reaction

Total RNA was extracted from mouse tissues using TRIzol (Invitrogen, California, CA) and mRNA was purified using Oligo-Tex (Takara Bio Inc., Tokyo, Japan). For detecting mRNA expression of the knock-in allele, RT-PCR was performed using mRNA extracted from hematopoietic tissues as described previously (Miyazaki et al., 2002). The primer sequences used for RT-PCR are shown in Supplemental information. GAPDH RT-PCR was also performed as an internal control. To examine Runx1 downstream target gene expression, quantitative RT-PCR was performed as described (Maki et al., 2005).

Western blot analysis

Nuclear extracts were isolated from whole embryos at 13.5 dpc or 16.5 dpc as previously described (Miyazaki et al., 2002). Western blot was performed using an anti-Runx1 antibody (Active Motif, Carlsbad, CA), an anti-Evi1 antibody (kindly provided by Dr. Morishita of Miyazaki University in Japan), or an anti-β-actin antibody (Millipore, Bedford, USA) according to the developer's and manufacturers' instructions.

Fetal liver cell preparation and colony formation assay

Fetal livers (FLs) were separated from 12.5 dpc embryos and mononuclear cells of each FL were collected and counted. Colony formation assay was performed using methylcellulose supplemented with EPO or a cocktail of cytokines as described previously (Nakahata and Ogawa, 1982; Ma et al., 2001). All the aggregates consisting of more than 50 cells were counted as colonies, except for magakaryocyte colonies, and colony types were determined on days 7 to 14 as described previously (Nakahata and Ogawa, 1982).

Flow cytometric analysis

Flow cytometric analyses of FL cells at 12.5 dpc were performed as reported (Ema et al., 2005; Morita et al., 2006). Detection of HSCs, common myeloid progenitors (CMPs), granulocyte/macrophage progenitors (GMPs), megakaryocyte/erythrocyte progenitors (MEPs), and common lymphocyte progenitors (CLPs) was performed using eight-parameter 6-color method with antibodies listed in Supplemental information on a FACS Canto II (BD Biosciences, San Jose, CA). Transplanted FL cells were analyzed with antibodies listed in Supplemental information on a FACS Calibur (BD Biosciences, San Jose, CA). The biotinylated antibody was developed with streptavidin (SA)-APC-Cy7 (BioLegend, San Diego, CA).

Analysis of apoptosis and cell cycle status

FL cells were prepared from 12.5 dpc embryos. 4.5×10^4 cells were cultured in αMEM (Sigma) containing 20% FBS, 100 ng/ml SCF, 10 ng/ml IL-3 and 10 ng/ml IL-6. Lineage-negative (lin^-), c-kit-positive ($c\text{-}kit^+$) cells were isolated using antibodies listed in Supplemental information. For detecting apoptotic cells, $lin^-c\text{-}kit^+$ cells were stained with anti-Annexin V-FITC and Annexin V^+ cells were analyzed using the Annexin V-FITC Apoptosis detection kit II, according to the manufacturer's instructions (BD Biosciences). For determining cell cycle status, $lin^-c\text{-}kit^+$ cells were stained with propidium iodide (PI), and the amount of nuclear DNA was measured using the CycleTEST PLUS DNA Reagent Kit, according to the manufacturer's instructions (BD Biosciences).

Competitive repopulation assay of FL cells

Competitive repopulation assay was performed using the Ly5 congenic mouse system. 2×10^5 FL cells from $Runx1^{+/+}$ or $Runx1^{\Delta IRES/\Delta IRES}$ embryos ($Ly5.2^+$) at 13.5 dpc were mixed with the same number of FL cells from a wild-type $Ly5.1^+$ embryo at the same age and were transplanted into irradiated (9.5 Gy) $Ly5.1^+$ recipient mice. Peripheral blood cells of the recipient mice were stained with anti-Ly5.1 and anti-Ly5.2 antibodies (see Supplemental information) for the percentage of $Ly5.2^+$ cells at 4, 8, and 12 weeks after transplantation. At 12 weeks after transplantation, the percentage of $Ly5.2^+$ cells was also analyzed on the thymus, spleen, and bone marrow in addition to the peripheral blood using anti-Ly5.1, anti-Ly5.2, and other lineage-specific antibodies (see Supplemental information).

Results

Generation of wild-type Runx1 knock-in mice deleted with the IRES element

A schematic representation of the regulatory elements controlling Runx1 expression at the level of transcription and translation is shown in Fig. 1A. A message transcribed from the P1 contains exon 1, which is spliced into the coding region of exon 3 to produce Runx1c,

whereas the P2-derived message initiates at exon 3 to produce Runx1b, which can be translated in both cap-dependent and IRES-mediated manners. We first investigated the role of the IRES in normal Runx1 function, by generating wild-type Runx1 knock-in mice, in which a part of the 5′ UTR containing the IRES element was deleted. For this purpose, the coding region of exon 3 and part of intron 3 were replaced with the complete human Runx1b cDNA (hRunx1b) fused at the 3′ end to a polyadenylation signal (pA) and flanked by two loxP sites, where the first loxP was designed to disrupt the IRES sequences (Fig. 1B). In these mice, the wild-type Runx1 was expressed by both the P1 and P2, but not by the IRES.

ES cells with homologous recombination, identified by 5′ genomic PCR and 3′ Southern blot (Fig. 1C, left and middle panels), were used to generate the knock-in mice ($Runx1^{+/KI}$). The Neo resistance gene was removed by the Flpe recombinase so as to avoid any effects of the Neo promoter on Runx1 expression (Fig. 1C, right panel). In the resultant mice ($Runx1^{+/\Delta IRES}$), as shown in Fig. 1B, P1-dependent Runx1c expression was retained, since the splicing acceptor site was conserved in the hRunx1b cDNA, and P2-dependent Runx1b expression was also unaffected, but IRES-dependent translation of the latter message was eliminated. The expression of the RNAs transcribed from the P1 and P2 within the knock-in allele was confirmed by performing reverse transcription polymerase chain reaction (RT-PCR) using primers derived from exons 1 (mRunx1c) and 3 (mRunx1b) along with a primer specific for hRunx1b (hRunx1-4) that does not anneal to the endogenous mouse Runx1 message (Fig. 1D). The expression of Runx1 protein in $Runx1^{+/+}$ and $Runx1^{\Delta IRES/\Delta IRES}$ mice was examined by blotting nuclear extracts of whole embryos with an anti-Runx1 antibody. As shown in Fig. 1E, comparable amount of Runx1 protein was detected in both types of mice. To further examine the distribution and amount of Runx1 protein in $Runx1^{+/+}$ and $Runx1^{\Delta IRES/\Delta IRES}$ embryos, sagittal sections of the embryos were immunohistochemically stained with an anti-Runx1 antibody. As shown in Supplemental Fig. 1, similar staining pattern and intensity were observed in both types of embryos. These results indicated that IRES deficiency did not significantly affect Runx1 protein expression during embryonic development.

Homozygotes expressing wild-type Runx1 deleted for the IRES ($Runx1^{\Delta IRES/\Delta IRES}$) died in utero at around 14.5 dpc, exhibiting vessel dilatation, subcutaneous edema, and pale liver

Heterozygous mice ($Runx1^{+/\Delta IRES}$) were indistinguishable from their wild-type littermates and were intercrossed to obtain homozygous mutants ($Runx1^{\Delta IRES/\Delta IRES}$). No live $Runx1^{\Delta IRES/\Delta IRES}$ mice were born, indicating that mice with deletion of the IRES element were embryonic lethal. Timed pregnancy revealed that $Runx1^{\Delta IRES/\Delta IRES}$ mice died *in utero* at approximately 14.5 dpc (Supplemental Table 1).

The representative macroscopic appearances and HE-stained sagittal sections of $Runx1^{+/+}$ and $Runx1^{\Delta IRES/\Delta IRES}$ embryos at 13.5 dpc are shown in Fig. 2A. As compared to $Runx1^{+/+}$ embryo, $Runx1^{\Delta IRES/\Delta IRES}$ embryo exhibited marked vessel dilatation mainly in the trunk, subcutaneous edema, and pale liver (indicated by arrows, an arrowhead, and a white triangle, respectively, in the right panels of Fig. 2A).

The results of microscopic analyses are shown in Fig. 2B. In contrast to the normal peripheral blood vessels of $Runx1^{+/+}$ mice (indicated by arrowheads in the left upper panel of Fig. 2B), those of $Runx1^{\Delta IRES/\Delta IRES}$ mice were markedly dilated and occasionally formed microaneurysms with hemorrhage (indicated by arrows in the right upper panel of Fig. 2B). In addition, as shown in the right middle panel of Fig. 2B, the subcutaneous region of $Runx1^{\Delta IRES/\Delta IRES}$ was highly edematous (shown as "Edema") and was associated with vessel dilatation and bleeding (indicated by an arrow). On the other hand, no obvious difference in blood vessel formation was observed in major internal organs of $Runx1^{+/+}$ and $Runx1^{\Delta IRES/\Delta IRES}$ embryos, such as the brain (indicated by arrowheads in the lower panels of Fig. 2B).

Capillary-associated pericytes were poorly developed in $Runx1^{\Delta IRES/\Delta IRES}$ mice

To investigate the mechanism(s) underlying vascular dilatation, capillaries were immunohistochemically stained with antibodies against vessel-related molecules. An antibody against α-smooth muscle actin (SMA) that detects pericytes gave rise to distinct differences in staining in $Runx1^{+/+}$ and $Runx1^{\Delta IRES/\Delta IRES}$ embryos, which correlated well with the distribution of vascular dilatation. Normal subcutaneous capillaries of $Runx1^{+/+}$ embryos were clearly stained with the anti-SMA antibody (indicated by arrowheads in the left upper panel of Fig. 2C), whereas the abnormally dilated subcutaneous vessels in $Runx1^{\Delta IRES/\Delta IRES}$ embryos were only faintly stained with the same antibody (indicated by arrows in the right upper panel of Fig. 2C). In contrast, capillaries in major organs, such as the brain, were stained to a similar extent with this antibody in both types of embryos (indicated by arrowheads in the lower panels of Fig. 2C). These results strongly suggested that dysfunction of capillary-associated pericytes was responsible for the vascular dilatation observed in $Runx1^{\Delta IRES/\Delta IRES}$ embryos. To investigate possible structural changes in the pericytes of the mutant mice, the subcutaneous peripheral blood vessels of $Runx1^{+/+}$ and $Runx1^{\Delta IRES/\Delta IRES}$ embryos were subjected to electron microscopic analysis. As shown in Fig. 2D, in contrast that the pericytes of $Runx1^{+/+}$ mice tightly attached and surrounded the endothelial cells (left panel), those of $Runx1^{\Delta IRES/\Delta IRES}$ mice were poorly developed, partly detached from the endothelial cells, and invaginated into the vessels (right panel). To ascertain whether Runx1 is expressed in pericytes, small and large vessels of $Runx1^{+/+}$ embryos were stained with an anti-Runx1 antibody. As shown in Fig. 2E, positive staining was detected in a cell morphologically resembling a pericyte and surrounding a capillary (indicated by an arrow in the right panel) but was not observed in a cell morphologically resembling a smooth muscle cell and lining inferior vena cava (indicated by an arrowhead in the right panel). These results indicate that Runx1 is preferentially expressed in pericytes among vessel-surrounding cells and that IRES-mediated Runx1 expression is essential for peripheral blood vessel integrity through effects on normal pericyte development and function during embryogenesis.

Marked reduction, altered differentiation, increased apoptosis, and decreased cell cycle of $Runx1^{\Delta IRES/\Delta IRES}$ FL hematopoietic cells

The $Runx1^{\Delta IRES/\Delta IRES}$ FL was hardly detectable through the skin (indicated by a white triangle in the right panels of Fig. 2A) and macroscopically looked very pale (right upper panel of Fig. 3A). Microscopic analysis revealed that $Runx1^{\Delta IRES/\Delta IRES}$ FL contained a significantly reduced number of hematopoietic cells, as compared to $Runx1^{+/+}$ FL (indicated by arrows in the right lower panel of Fig. 3A). The marked reduction in cell number was further demonstrated by cell counting of $Runx1^{+/+}$, $Runx1^{+/\Delta IRES}$, and $Runx1^{\Delta IRES/\Delta IRES}$ FLs (Fig. 3B).

We then investigated the differentiation status of $Runx1^{+/+}$ and $Runx1^{\Delta IRES/\Delta IRES}$ FL hematopoietic cells. A detailed FACS analysis using a 6-colored method was applied, which detects hematopoietic cells with various differentiation stages, including hematopoietic stem cell (HSC), common myeloid progenitor (CMP), granulocyte/macrophage progenitor (GMP), megakaryocyte/erythrocyte progenitor (MEP), and common lymphocyte progenitor (CLP) fractions. As shown in Fig. 3C, although the total cell number in $Runx1^{\Delta IRES/\Delta IRES}$ FL was significantly reduced as compared to that in $Runx1^{+/+}$ FL, all the fractions were present in both

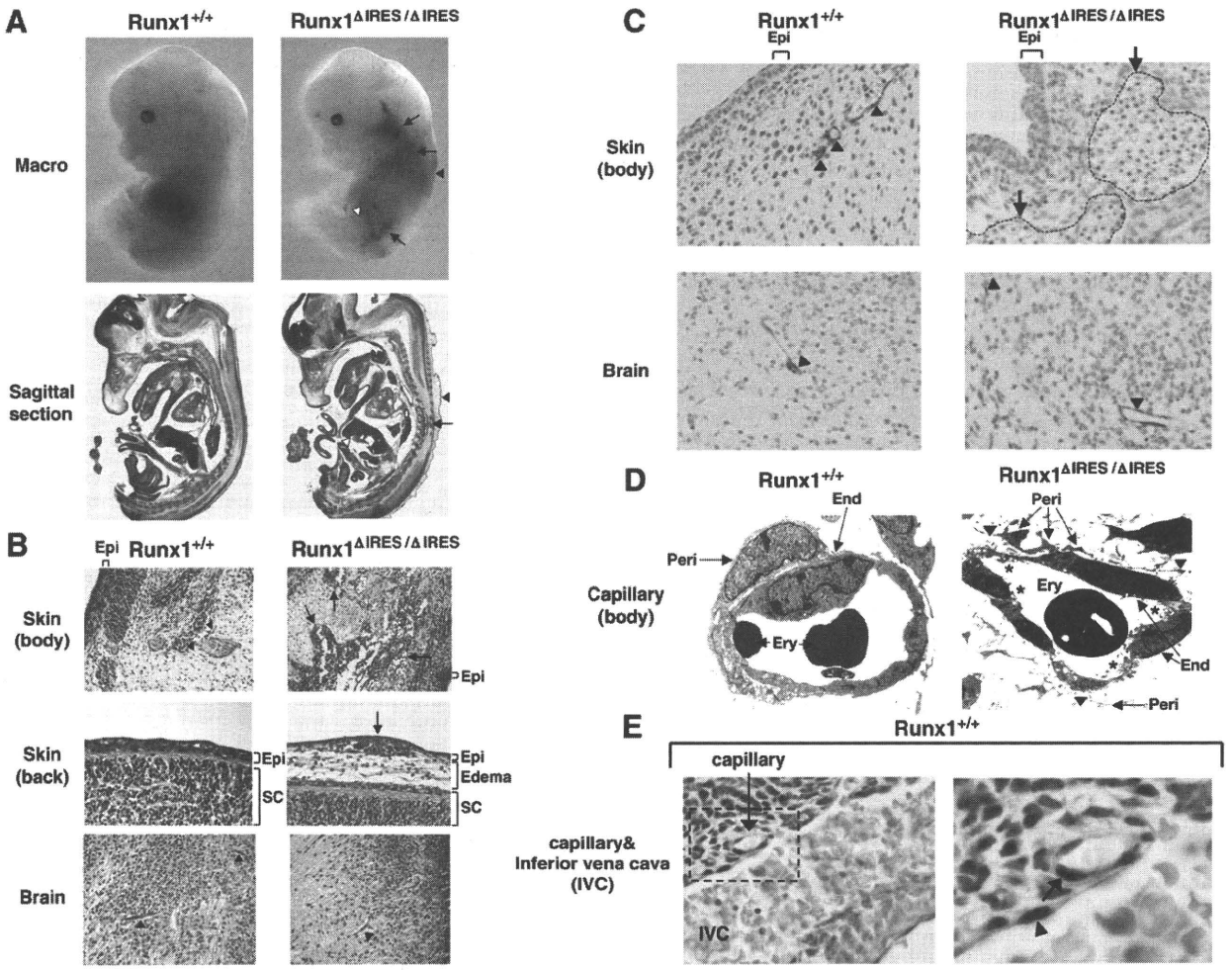

Fig. 2. Pathological analyses of Runx1$^{+/+}$ and Runx1$^{\Delta IRES/\Delta IRES}$ embryos. (A) Macroscopic appearances (upper panels) and HE-stained sagittal sections (lower panels) at 13.5 dpc. Prominently dilated subcutaneous blood vessels and subepidermal edema are indicated by arrows and an arrowhead, respectively, and pale liver is indicated by a white triangle (also see Fig. 3A). (B) HE-stained tissue sections at 13.5 dpc. Normal and dilated capillaries are indicated by arrowheads and arrows, respectively. In the skin sections (body and back, upper and middle panels), vascular dilatation with hemorrhage and subepidermal edema (Edema) are apparent in Runx1$^{\Delta IRES/\Delta IRES}$ embryos. In contrast, in the brain sections (lower panels), no dilated vessels are observed in both types of embryos. Epi, epidermis; SC, spinal cord. (C) Immunohistochemical staining with an anti-SMA antibody at 13.5 dpc. In the skin sections (body, upper panels), positive staining is detected around normal capillaries in Runx1$^{+/+}$ embryos (indicated by arrowheads), whereas no staining is observed around the dilated capillaries (indicated by dotted lines) in Runx1$^{\Delta IRES/\Delta IRES}$ embryos (indicated by arrows). In contrast, in the brain sections (lower panels), staining of a similar intensity is observed in both types of embryos (indicated by arrowheads). Epi, epidermis. (D) Electron microscopic analysis of capillaries at 13.5 dpc. In a Runx1$^{+/+}$ capillary, a pericyte (Peri) tightly attaches and surrounds an endothelial cell (End) (left panel). In contrast, in a Runx1$^{\Delta IRES/\Delta IRES}$ capillary, pericytes are partly detached from endothelial cells (indicated by arrowheads in the right panel) and are invaginated into vessels with enlarged pinocytotic vesicles (indicated by asterisks in the right panel). Ery, erythrocyte. (E) Immunohistochemical staining with an anti-Runx1 antibody at 14.5 dpc. The boxed area in the left panel is magnified in the right panel. In the right panel, positive staining is detected in a pericyte-like cell surrounding a capillary (indicated by an arrow) but not observed in a smooth muscle-like cell lining inferior vena cava (IVC) (indicated by an arrowhead).

types of mice. No significant change was observed in the HSC fraction (2.08% in Runx1$^{+/+}$ FL and 3.81% in Runx1$^{\Delta IRES/\Delta IRES}$ FL, Fig. 3C upper panels), whereas a decrease in MEP fraction and an increase in CMP and GMP fractions were observed in Runx1$^{\Delta IRES/\Delta IRES}$ FL as compared to Runx1$^{+/+}$ FL (percentages of Runx1$^{+/+}$ FL and Runx1$^{\Delta IRES/\Delta IRES}$ FL were; 94.9% and 41.6% for MEP, 3.04% and 30.2% for CMP, and 0.53% and 3.1% for GMP, Fig. 3C middle panels). As for CLP, although a slight increase was observed in Runx1$^{\Delta IRES/\Delta IRES}$ FL (7.17% in Runx1$^{+/+}$ FL and 19.4% in Runx1$^{\Delta IRES/\Delta IRES}$ FL, Fig. 3C lower panels), the difference was not reproducible, due to the limited number of cells present in this fraction at this stage.

We next analyzed the apoptotic state and cell cycle profile of the Runx1$^{+/+}$ and Runx1$^{\Delta IRES/\Delta IRES}$ FL hematopoietic stem/early progenitor cells. Lineage-negative (lin$^-$), c-kit-positive (c-kit$^+$) cells were

Fig. 3. Hematopoietic analysis of Runx1$^{+/+}$ and Runx1$^{\Delta IRES/\Delta IRES}$ FLs. (A) Macroscopic appearances (upper panels) and HE-stained sections (lower panels) of Runx1$^{+/+}$ and Runx1$^{\Delta IRES/\Delta IRES}$ FLs at 12.5 dpc. As compared to Runx1$^{+/+}$ FL, Runx1$^{\Delta IRES/\Delta IRES}$ FL is pale and contains significantly reduced number of hematopoietic cells (indicated by arrows). (B) Comparison of FL cell numbers among Runx1$^{+/+}$, Runx1$^{+/\Delta IRES}$, and Runx1$^{\Delta IRES/\Delta IRES}$ embryos at 12.5 dpc. Data are plotted as means with error bars. A significant reduction in the cell number is observed in Runx1$^{\Delta IRES/\Delta IRES}$ FL ($p<0.01$). (C) Flow cytometric analysis of HSC and progenitor fractions of Runx1$^{+/+}$ and Runx1$^{\Delta IRES/\Delta IRES}$ FLs at 12.5 dpc. MEP, megakaryocyte/erythrocyte progenitor; GMP, granulocyte/macrophage progenitor; CMP, common myeloid progenitor; and CLP, common lymphocyte progenitor. As compared to Runx1$^{+/+}$ FL, Runx1$^{\Delta IRES/\Delta IRES}$ FL shows an increase in GMP and CMP fractions but a decrease in MEP fraction. (D) Apoptotic state and cell cycle profile of the Runx1$^{+/+}$ and Runx1$^{\Delta IRES/\Delta IRES}$ FL hematopoietic stem/early progenitor cells at 12.5 dpc. Data are plotted as means with error bars. As compared to Runx1$^{+/+}$ FL, Runx1$^{\Delta IRES/\Delta IRES}$ FL shows an increase in Annexin V$^+$ apoptotic cells (upper panel, $p=0.15$) and a decrease in S-G_2/M cycling cells (lower panel, $p=0.07$).

isolated from Runx1$^{+/+}$ and Runx1$^{\Delta IRES/\Delta IRES}$ FLs, stained with Annexin V or propidium iodide (PI), and analyzed by FACS. As shown in Fig. 3D, as compared to lin$^-$c-kit$^+$ cells of Runx1$^{+/+}$ FL, those of Runx1$^{\Delta IRES/\Delta IRES}$ FL exhibited an increase in the percentage of apoptotic Annexin V$^+$ cells (upper panel) and a decrease in the proportion of cycling (S-G_2/M phase) cells (lower panel), although

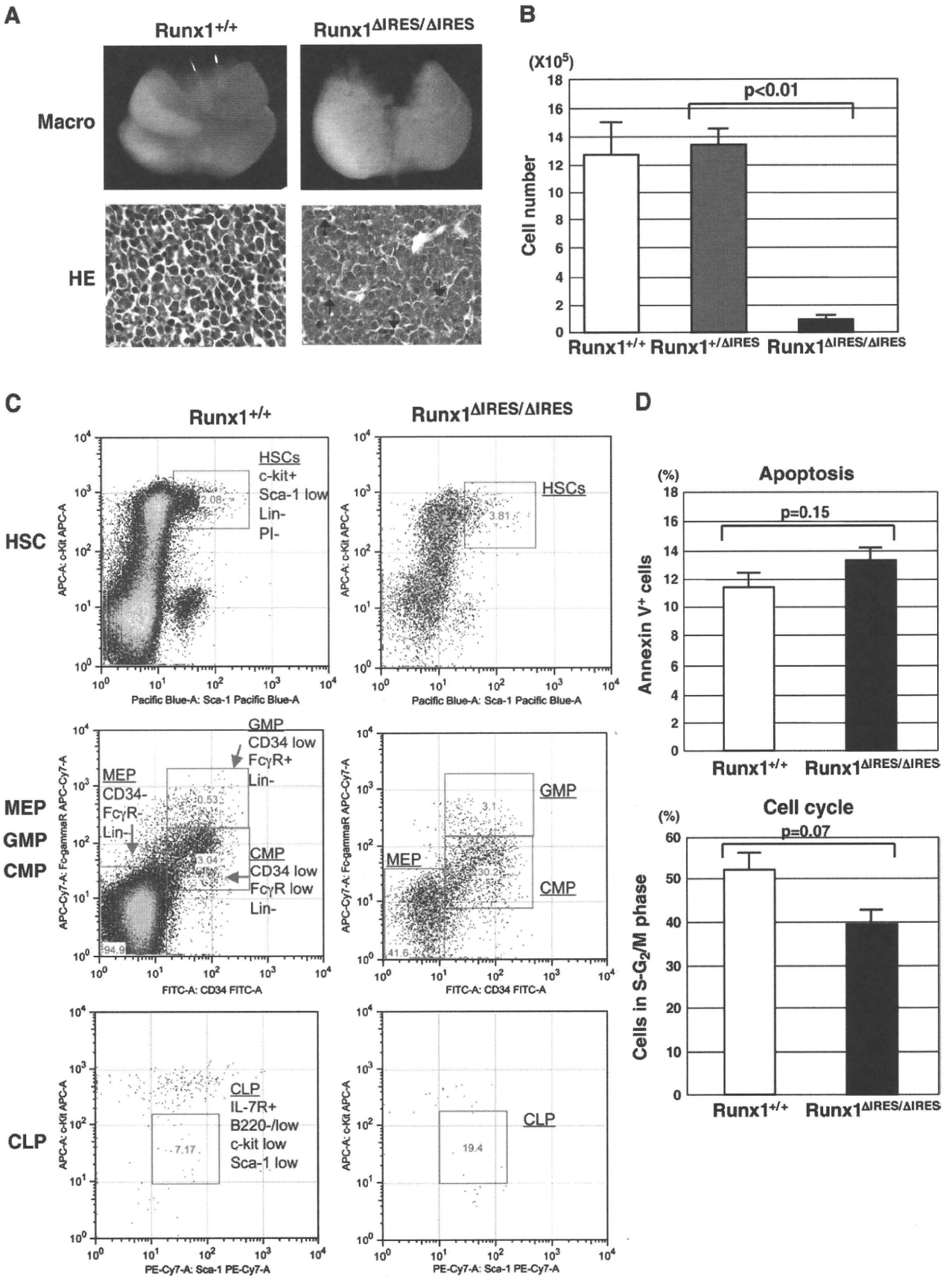

the differences were not statistically significant ($p = 0.15$ for apoptotic analysis and $p = 0.07$ for cell cycle analysis).

These results indicated that IRES-mediated Runx1 expression is pivotal in expansion of FL hematopoietic cells and affected differentiation, apoptotic status, and cell cycle profile.

Reduced colony formation activity and altered expression of downstream target genes in Runx1$^{\Delta IRES/\Delta IRES}$ FL hematopoietic cells

We then rigorously evaluated the proliferative potential of Runx1$^{\Delta IRES/\Delta IRES}$ FL hematopoietic cells. We first examined the colony-forming activity by culturing FL hematopoietic cells of Runx1$^{\Delta IRES/\Delta IRES}$ mice and their control (Runx1$^{+/+}$ and Runx1$^{+/\Delta IRES}$) littermates with various cytokines. As shown Table 1, hematopoietic CFUs generated from Runx1$^{\Delta IRES/\Delta IRES}$ FL cells were markedly reduced as compared to those from control littermates. A significant decrease (80–90%) was observed in CFU-E and CFU-Mix colonies, while the reduction of BFU-E and CFU-GM colonies was less remarkable (~50%). In addition, although single megakaryocytes were occasionally observed, no megakaryocytic colonies were generated from Runx1$^{\Delta IRES/\Delta IRES}$ FLs. Moreover, Runx1$^{\Delta IRES/\Delta IRES}$ FL-derived colonies were smaller and contained fewer cells than control FL-derived colonies (Supplemental Fig. 2).

To investigate the molecular mechanisms underlying the altered proliferative activity in Runx1$^{\Delta IRES/\Delta IRES}$ FLs, we examined the expression patterns of Runx1 downstream target genes implicated in definitive hematopoiesis. RNAs extracted from Runx1$^{+/+}$ and Runx1$^{\Delta IRES/\Delta IRES}$ FLs were subjected to quantitative RT-PCR analysis. The expression levels of the indicated genes in Runx1$^{\Delta IRES/\Delta IRES}$ FL relative to those in Runx1$^{+/+}$ FL are shown in Fig. 4. Although all the genes examined were expressed in both Runx1$^{+/+}$ and Runx1$^{\Delta IRES/\Delta IRES}$ FLs, the expression levels varied among genes. Enhanced expression was detected for CEBPα, M-CSFR, and G-CSFR, while reduced expression was observed for NFE2, β-globin, ALAS-E, and MPO in Runx1$^{\Delta IRES/\Delta IRES}$ FL as compared to Runx1$^{+/+}$ FL.

Impaired repopulation ability of Runx1$^{\Delta IRES/\Delta IRES}$ FL cells in the competitive repopulation assay

We nest investigated the *in vivo* repopulation ability of Runx1$^{\Delta IRES/\Delta IRES}$ FL cells, by performing the competitive repopulation assay using the Ly5 congenic mouse system. Irradiated Ly5.1^{+} mice were transplanted with FL cells from a Runx1$^{+/+}$ or a Runx1$^{\Delta IRES/\Delta IRES}$ embryo (Ly5.2^{+}) together with the same number of FL cells from a wild-type Ly5.1^{+} embryo of the same age. Engraftment of the Runx1$^{+/+}$ or Runx1$^{\Delta IRES/\Delta IRES}$ FL-derived cells was analyzed by flow cytometry and the repopulation ratio was assessed as the percentage of Ly5.2^{+} cells in the peripheral blood (PB) (4, 8, and 12 weeks after transplantation) and in the hematopoietic tissues (12 weeks after transplantation). The analysis of the PB showed that the overall reconstitution ability of Runx1$^{\Delta IRES/\Delta IRES}$ FL was significantly reduced as compared to that of Runx1$^{+/+}$ FL (left panel of Fig. 5A). Interestingly, while the reconstitution ability in granulocytes was not significantly affected (middle panel of Fig. 5A), that in lymphocytes was severely impaired (right panel of Fig. 5). In addition, the analysis of the hematopoietic tissues exhibited poor contribution of Runx1$^{\Delta IRES/\Delta IRES}$ FL cells, especially in the thymus and spleen (left panel of Fig. 5B). The cell lineage-specific analyses in the thymus, spleen, and BM revealed that Runx1$^{\Delta IRES/\Delta IRES}$ FL cells possessed a comparable reconstitution ability in myelomonocytic and megakaryocytic lineages (Gr1^{+}, Mac1^{+}, and CD61^{+} in the right panel of Fig. 5B), but exhibited a remarkably reduced reconstitution ability in T- and B-lymphoid lineages (Thy1.2^{+} and B220^{+} in the right panel of Fig. 5B). These results indicated that the repopulation ability of Runx1$^{\Delta IRES/\Delta IRES}$ FL hematopoietic cells was impaired, especially in the lymphoid lineages.

Heterozygotes expressing Runx1/Evi1 deleted with the IRES element were normally born and did not show any hematological abnormalities

We finally investigated the role of the IRES in leukemogenesis mediated by the expression of Runx1-fusion proteins. Runx1/Evi1 (RE), a Runx1 fusion protein created by t(3;21)(q26;q22) in human leukemia (Mitani et al., 1994), was knocked into the Runx1 locus, using a similar knock-in strategy as was used to generate Runx1$^{+/\Delta IRES}$, except that the Runx1/Evi1 cDNA fused to the pA was preceded by a floxed Neo resistance cassette (Fig. 6A). We generated RE knock-in mice, following removal of the Neo resistance cassette from the recombinant ES cells by Cre recombinase. The P1-derived RE message was expressed in these mice, since the splice acceptor site was conserved in the Runx1 region of RE. In addition, P2-dependent RE expression was unaffected, but IRES-dependent RE expression was eliminated (Runx1$^{+/RE\Delta IRES}$, Fig. 6A).

Correctly targeted ES cells identified by 5′ genomic PCR and 3′ Southern blot (Fig. 6B, left and middle panels) were used to generate knock-in mice following removal of the Neo resistance gene (Fig. 6B, right panel). The expression of the RE mRNAs from both the P1 and P2 promoters was confirmed by RT-PCR, using the same methods as used for the analysis of expression in the Runx1$^{+/RE\Delta IRES}$ mice (Fig. 6C). In addition, expression of RE protein in Runx1$^{+/RE\Delta IRES}$ mice was detected by Western blot (Fig. 6D).

Interestingly, in contrast to the conventional RE knock-in mice, which died *in utero* exhibiting CNS hemorrhage due to a dominant negative effect of RE on endogenous Runx1 function (Maki et al., 2005), Runx1$^{+/RE\Delta IRES}$ mice were born at the expected Mendelian ratio without any phenotypical defects (data not shown). In addition, no obvious differences in hematopoietic parameters were found between Runx1$^{+/+}$ and Runx1$^{+/RE\Delta IRES}$ mice during a long-term observation period (Fig. 6E), in contrast that conventional RE knock-in chimeric mice develop megakaryocytic leukemia (Maki et al., 2006). These results demonstrated that IRES-mediated RE expression was required for the dominant negative activity during embryogenesis and the leukemogenic potential in adult hematopoiesis.

Discussion

Runx1 is a gene whose expression is regulated transcriptionally by two distinct promoters (P1 and P2), giving rise to two different mRNAs, and also translationally by an IRES element, existing just upstream of the translation initiation codon of P2-derived mRNA (Pozner et al., 2000; Levanon and Groner, 2004). In this study, we applied a knock-in strategy to clarify the biological role(s) of the IRES sequences in normal Runx1-mediated hematopoiesis and angiogenesis and also in mutated Runx1-induced leukemogenesis.

We first generated knock-in mice of Runx1b, the predominant transcript of the Runx1 gene, in which promoter-dependent transcription was retained but IRES-medicated translation was eliminated. A number of Runx1 mRNAs are produced by alternative splicing (Levanon et al., 2001), while Runx1$^{\Delta IRES/\Delta IRES}$ mice generated Runx1c and IRES-disrupted Runx1b transcripts (Fig. 1B), raising the possibility that the phenotypes of our mutant mice might be due to the lack of the splice variants. However, our previous study demonstrated that mice containing Runx1b cDNA knocked into exon 4 of the Runx1 gene, which express Runx1c and Runx1b, developed normally and did not show any obvious defects (Okuda et al., 2000). Thus, the expression of Runx1c and Runx1b without other spliced forms is shown to be sufficient for the proper mouse development. The major difference in the regulatory elements controlling Runx1 expression between our previous and current studies is that Runx1b mRNA in this study lacks the IRES element. Therefore, the abnormal phenotypes observed in Runx1$^{\Delta IRES/\Delta IRES}$ mice are considered not due to the lack of alternatively spliced forms but to the lack of IRES-mediated Runx1 expression. However, as compared to the knock-in mice in our previous study (Okuda et al., 2000),

Table 1
Hematopoietic colony-forming activity of Runx1$^{+/+}$, Runx1$^{+/\Delta IRES}$, and Runx1$^{\Delta IRES/\Delta IRES}$ fetal livers.

Genotype	Cell counts/liver ($\times 10^5$)	Absolute number per fetal liver					
		CFU-E	BFU-E	CFU-Meg	CFU-GM	CFU-Mix	Total CFU-cells
+/+	12.60 ± 7.5 (n = 4)	58867	2495	1373	14301	2003	79040 (n = 4)
+/ΔIRES	13.67 ± 7.2 (n = 17)	59054	2556	1080	16021	3158	81883 (n = 5)
ΔIRES/ΔIRES	2.02 ± 0.6 (n = 7)	3024	1091	0	7123	436	11684 (n = 6)
Ratio for cut-down $\left(\frac{+/+ -\Delta IRES/\Delta IRES}{+/+}\right)$	84.0%	94.9%	56.3%	100%	50.2%	78.2%	85.2%

1×10^4 MNCs from each single fetal liver at 12.5 dpc were initially plated in 1 ml semisolid cultures with cytokine cocktail.
Colony types and numbers were determined at days 10 to 15 in the culture. Table shows converted absolute CFU cell numbers per fetal liver.

Runx1$^{\Delta IRES/\Delta IRES}$ mice lack intron 3 in addition to the IRES element. Thus, there remains the possibility that intron 3 contains an element with an enhancer activity that affects Runx1 function.

Runx1$^{\Delta IRES/\Delta IRES}$ mice died *in utero* at around 14.5 dpc (Supplemental Table 1) with prominently dilated peripheral capillaries, severe subepidermal edema, and pale liver (Figs. 2A and B), which demonstrated the indispensable role of the IRES element in embryonic development. To investigate the effect of the deletion of the IRES on Runx1 expression, we performed western blot and immunohistochemical staining of Runx1$^{+/+}$ and Runx1$^{\Delta IRES/\Delta IRES}$ embryos. As shown in Fig. 1E and Supplemental Fig. 1, both types of embryos exhibited comparable amounts and similar distribution patterns of Runx1 protein, indicating that IRES deficiency did not significantly affect the Runx1 protein expression. This finding led us to the idea that IRES-mediated Runx1 expression might be essential in a specific developmental stage, a particular cell lineage and/or a critical point of cell cycle, as suggested in previous studies (Mitchell et al., 2003; Gonzalez-Herrera et al., 2006; Audigier et al., 2008; Dobbyn et al., 2008; Jo et al., 2008).

Interestingly, the phenotype and death period of Runx1$^{\Delta IRES/\Delta IRES}$ mice differ from those of Runx1 full-knockout (Runx1$^{-/-}$) mice. Runx1$^{-/-}$ mice die of CNS hemorrhage at around 12.5 dpc (Okuda et al., 1996; Wang et al., 1996; Okada et al., 1998), whereas Runx1$^{\Delta IRES/\Delta IRES}$ mice survive this stage and presumably die of circulation failure at around 14.5 dpc. Although the reason for the phenotypical and temporal differences in the embryonic lethality of these mutant mice is not clear yet, it could be postulated that P1- and P2-derived Runx1 expression in a cap-dependent fashion rescues Runx1$^{\Delta IRES/\Delta IRES}$ mice from the fatal CNS hemorrhage at earlier stages but cannot prevent vessel dilatation, fluid leakage and circulation failure at later stages, when IRES-mediated Runx1 expression is absolutely required. In addition, it is intriguing that Runx1$^{\Delta IRES/\Delta IRES}$ mice die earlier than P2-specific knockdown (P2$^{neo/neo}$) mice that develop to term (Pozner et al., 2007; Bee et al., 2010), since the IRES is coupled to P2-derived mRNA (Fig. 1A). One possible explanation for this discrepancy is that P2 activity is not completely eliminated in the knockdown system and the residual P2-derived transcript rescues P2$^{neo/neo}$ embryos from fatal vessel dilatation and systemic edema observed in Runx1$^{\Delta IRES/\Delta IRES}$ embryos.

It is of note that the blood vessel dilatation in Runx1$^{\Delta IRES/\Delta IRES}$ mice was prominent in the trunk but was not observed in major organs, such as the brain (Figs. 2A and B). These results indicated that the Runx1 IRES plays a region-preferential role in vascular development. The underlying mechanism is not clear, but one possibility is the difference in the oxygen partial pressure (PO_2) among organs. A previous report showed that during embryonic development, the mean PO_2 in the head is significantly higher than that in the trunk (Meuer et al., 1992). Given that IRES-mediated translation predominates under hypoxic conditions (Stoneley and Willis, 2004; Holcik and Sonenberg, 2005), it could be postulated that IRES-mediated Runx1 expression plays a more substantial role in the trunk than in the brain, which underlies the peripheral tissue-predominant vascular dilatation in Runx1$^{\Delta IRES/\Delta IRES}$ mice.

The immunohistochemical analysis showed that Runx1 is preferentially expressed in capillary-associated pericytes (Fig. 2E) and the electron microscopic analysis revealed that pericytes in Runx1$^{\Delta IRES/\Delta IRES}$ embryos were poorly developed (Fig. 2D). Pericytes surround the vascular endothelial cells and maintain the integrity of blood vessels (Kubo and Alitalo, 2003). In addition, pericytes produce angiopoietin-1, a factor promoting angiogenesis by binding to Tie2 receptors expressed on

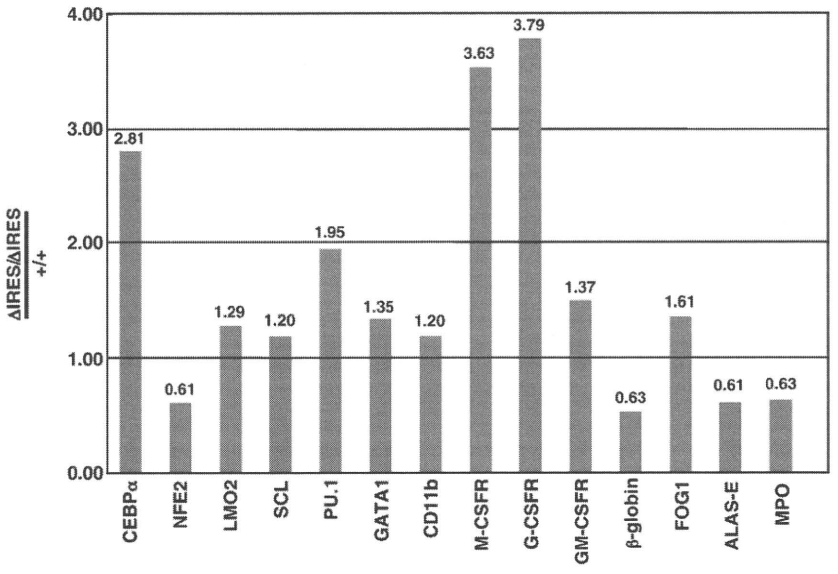

Fig. 4. Expression changes of Runx1 downstream target genes. RNAs extracted from Runx1$^{+/+}$ and Runx1$^{\Delta IRES/\Delta IRES}$ FLs at 12.5 dpc were subjected to quantitative RT-PCR. The expression levels of the genes in Runx1$^{\Delta IRES/\Delta IRES}$ FL relative to those in Runx1$^{+/+}$ FL are shown. Data are plotted as means of three independent mice.

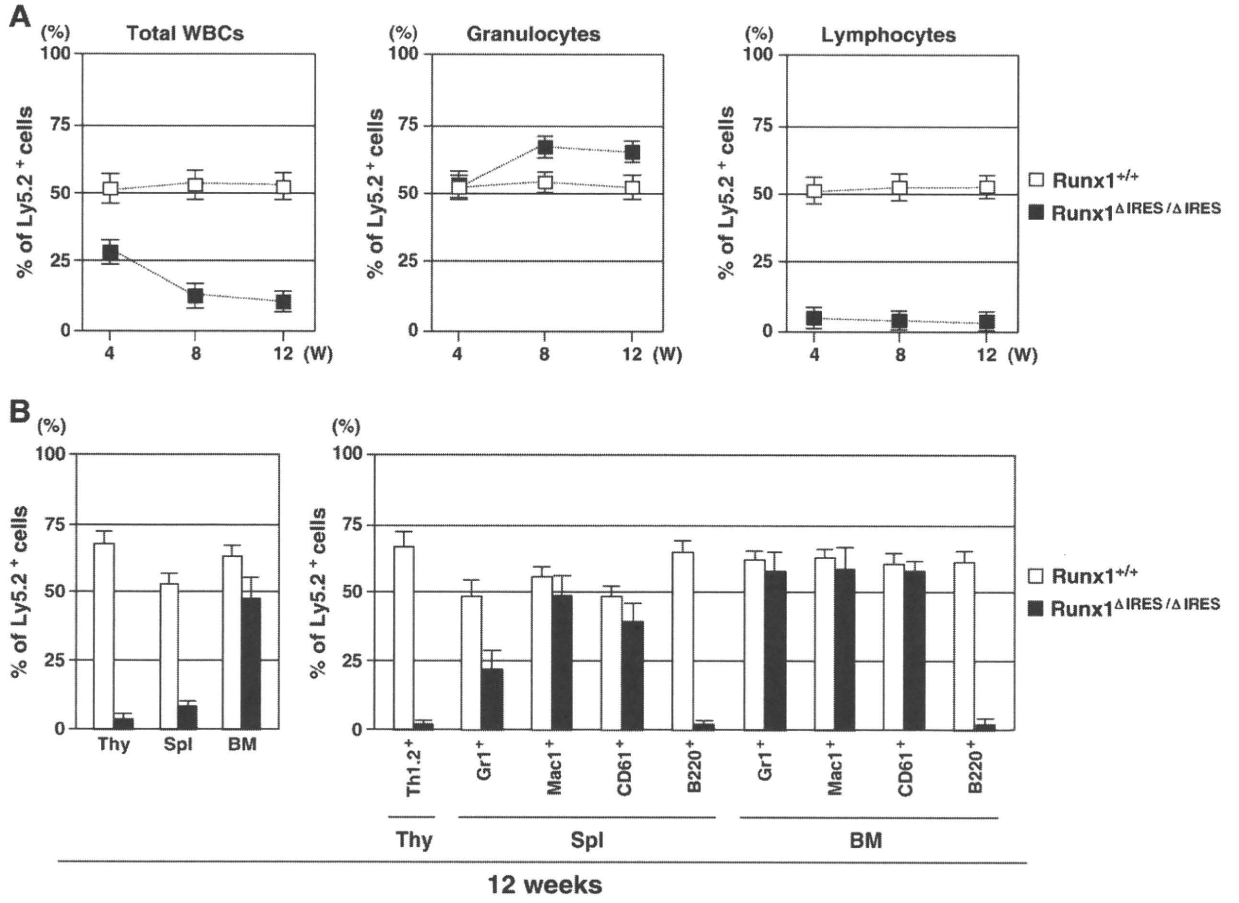

Fig. 5. Repopulation ability of Runx1$^{+/+}$ and Runx1$^{\Delta IRES/\Delta IRES}$ FL cells. (A) Contribution of donor-derived cells to the peripheral blood of the recipient mice at 4, 8, and 12 weeks after transplantation. The percentages of Runx1$^{+/+}$ (white boxes) and Runx1$^{\Delta IRES/\Delta IRES}$ (black boxes) cells (Ly5.2^{+}) in the total WBCs, granulocytes, and lymphocytes are shown. Data are plotted as means with error bars. (B) Contribution of donor-derived cells to the thymus (Thy), spleen (Spl), and bone marrow (BM) of the recipient mice at 12 weeks after transplantation. The percentages of Runx1$^{+/+}$ (white boxes) and Runx1$^{\Delta IRES/\Delta IRES}$ (black boxes) cells (Ly5.2^{+}) in the thymus, spleen, and bone marrow (left panel) and in various hematopoietic lineages in these tissues (right panel) are shown. Data are plotted as means with error bars.

endothelial cells (Davis et al., 1996). Thus, pericytes contribute to blood vessel formation through structurally stabilizing vascular architecture and functionally promoting vascular remodeling. These findings strongly suggest that Runx1 plays an important role in pericyte development, as suggested in previous studies (Lacaud et al., 2002; Kubo and Alitalo, 2003) and that Runx1 IRES deficiency directly impaired pericyte function and led to the vascular abnormalities observed in Runx1$^{\Delta IRES/\Delta IRES}$ mice.

Another remarkable aspect of Runx1$^{\Delta IRES/\Delta IRES}$ mice was pale liver, due to a significant reduction of hematopoietic cells (Figs. 2A and 3A and B). This finding indicated that IRES-mediated Runx1 expression is pivotal not only for vascular development but also for FL hematopoiesis. The mechanism underling the reduction of Runx1$^{\Delta IRES/\Delta IRES}$ FL hematopoietic cells is not clear, but Runx1$^{\Delta IRES/\Delta IRES}$ hematopoietic stem/early progenitor cells exhibited an increased ratio of apoptosis and a decreased ratio of cell cycling (Fig. 3D). Therefore, it seems likely that these abnormalities would be, at least partly, responsible for the poor proliferation of Runx1$^{\Delta IRES/\Delta IRES}$ FL hematopoietic cells.

It is to be noted that the differentiation and proliferation activities of Runx1$^{\Delta IRES/\Delta IRES}$ FL cells varied among hematopoietic lineages. In the FACS analysis, the MEP fraction was markedly decreased, whereas the CMP and GMP fractions were relatively increased (Fig. 3C). In addition, in the colony formation assay, colony numbers of CFU-E and CFU-Meg were more significantly reduced than that of CFU-GM (Table 1). Quantitative RT-PCR analysis revealed that expression patterns of Runx1 target genes were altered in the Runx1$^{\Delta IRES/\Delta IRES}$ FL (Fig. 4). Downregulation of erythroid- and megakaryo-related genes (NFE2, β-globin, ALAS-E, and MPO) would be responsible for the marked reduction in MEP fraction and CFU-E and CFU-Meg colonies, and upregulation of myeloid- and macrophage-related genes (CEBPα, M-CSFR, and G-CSFR) would account for the less significant reduction of CMP and GMP fractions and CFU-GM colony. Moreover, in a competitive repopulation assay, Runx1$^{\Delta IRES/\Delta IRES}$ FL cells differentiated into myeloid lineages to a similar extent as Runx1$^{+/+}$ FL cells, but contributed to lymphoid lineages to a much lesser extent (Fig. 5). These results indicated that IRES-mediated Runx1 expression plays an essential role in expansion and differentiation of lymphoid cells. Interestingly, hematopoietic cells of Runx1 conditional knockout mice showed a similar phenotype; in the competitive repopulation assay, hematopoietic cells with acquired Runx1 ablation possessed an ability of myeloid differentiation but exhibited almost a complete lack of lymphoid differentiation (Ichikawa et al., 2004; Growney et al., 2005; Putz et al., 2006). These results strongly suggest that IRES-mediated expression plays substantial roles in Runx1 function not only in embryonic development but also in adult hematopoiesis.

We finally investigated the pathological role of the IRES in mutated Runx1-induced leukemia, by generating Runx1/Evi1 (RE) knock-in mice, in which promoter-dependent transcription was retained but IRES-mediated translation was eliminated (Runx1$^{+/RE\Delta IRES}$). Interestingly, although the RE protein was expressed in Runx1$^{+/RE\Delta IRES}$ mice (Fig. 6D), probably by a cap-dependent mechanism, the mice were normally born and did not exhibit any hematopoietic abnormalities during a long-term observation period (Fig. 6E). These results contrast

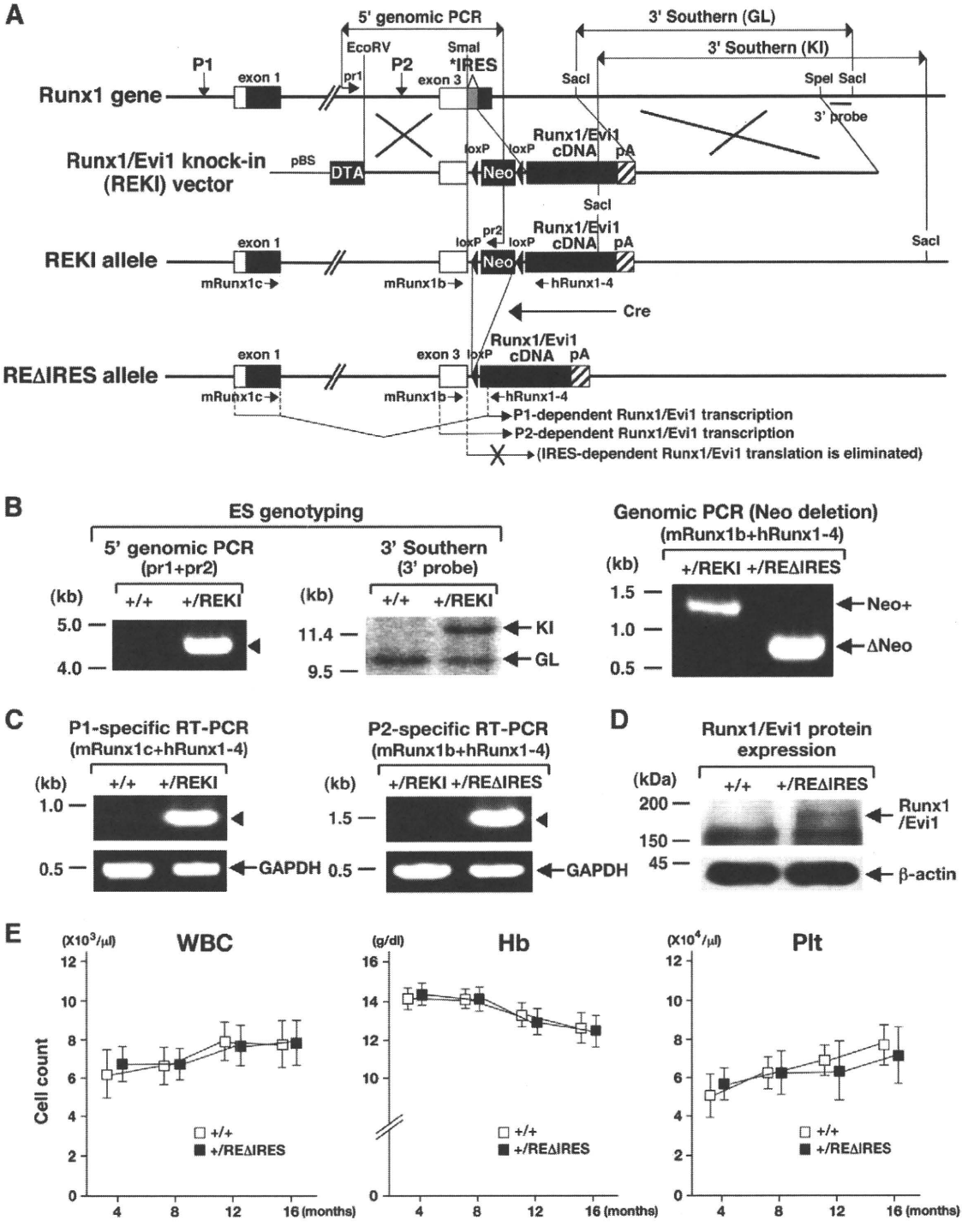

Fig. 6. Generation and analysis of Runx1/Evi1 (RE) knock-in mice deleted with the IRES element (Runx1$^{+/RE\Delta IRES}$). (A) Strategy for generating Runx1$^{+/RE\Delta IRES}$ mice. The knock-in strategy was essentially the same as that used in generating Runx1$^{+/\Delta IRES}$ embryos (Fig. 1B). In the Runx1$^{+/RE\Delta IRES}$ mice, P1- and P2-dependent RE transcription was retained, but IRES-mediated RE translation was eliminated. (B) Results of ES genotyping (left and middle panels) and removal of Neo resistance cassette (right panel). For ES genotyping, a positive PCR product for 5′ PCR is indicated by an arrowhead, and positions of germline (GL)- and KI-derived fragments for 3′ Southern blot are indicated by arrows. For Neo deletion, positions of Neo-positive (Neo+) and Neo-deleted (ΔNeo) PCR products are indicated by arrows. (C) RT-PCR analysis of the mRNA expression from the REΔIRES allele. The RT-PCR products are indicated by arrowheads (upper panels) and the GAPDH RT-PCR was performed as an internal control (lower panels). (D) Expression of RE protein. Nuclear extracts of Runx1$^{+/+}$ and Runx1$^{+/RE\Delta IRES}$ at 16.5 dpc were blotted with an anti-Evi1 (upper panel) or an anti-β-actin antibody (lower panel). (E) Changes in peripheral blood cell parameters in Runx1$^{+/+}$ (white boxes) and Runx1$^{+/RE\Delta IRES}$ (black boxes) mice at 4, 8, 12, and 16 months of age. Data are plotted as means with error bars.

previous studies that showed conventional RE knock-in heterozygotes died *in utero* at around 12.5 dpc due to CNS hemorrhage and RE knock-in chimeric mice developed megakaryoblastic leukemia (Maki et al., 2005; Maki et al., 2006). Therefore, although we did not directly compare the expression level of RE protein in the hematopoietic compartment between Runx1$^{+/RE\Delta IRES}$ and conventional RE knock-in mice, these results indicate that IRES-mediated translation is required for RE to exert its dominant negative activity during embryogenesis and leukemogenic potential in adult hematopoiesis.

In this study, we investigated the biological roles of the IRES element in the Runx1 gene and demonstrated that the region is essential for normal Runx1-mediated angiogenesis and hematopoiesis and also for a

Runx1 fusion protein-induced leukemogenesis. These results provide novel insights into the *in vivo* function of an IRES under physiological and pathological conditions, and demonstrate that this IRES-ablating gene targeting will find application in the elucidation of the biological roles of various cellular IRESes. In addition, since IRES-mediated translation has been shown to play an important role in tumorigenesis (Stoneley and Willis, 2004), our results raise the possibility that Runx1 IRES could be regarded as a potential therapeutic target for mutated Runx1-induced hematopoietic malignancies.

Author contributions

Akiko Nagamachi, Phyo Wai Htun, Feng Ma, Kazuko Miyazaki, Norimasa Yamasaki, Masamoto Kanno, Zen-ichiro Honda, Tsukasa Okuda, and Hiroaki Honda designed and performed the research and wrote the manuscript; Hideaki Oda centralized the pathological analysis; Feng Ma, and Kohichiro Tsuji participated in the flow cytometric and colony formation assays; and Akiko Nagamachi, Phyo Wai Htun, and Toshio Inaba performed the FL transplantation experiments. All the authors checked the final version of the manuscript.

Acknowledgments

We thank Yuki Sakai, Kayoko Hashimoto, Yuko Tsukawaki, and Rika Tai for mouse care and technical assistance, Masaki Miyazaki for the help in FACS analysis, Mutsuhiro Watanabe for the pathological analysis, Kazuhiro Morishita for an anti-Evi1 antibody, Nobuaki Yoshida for the E14 ES cells, and Hisamaru Hirai for the Runx1/Evi1 cDNA. This work was supported by a Grant-in-Aid from the Ministry of Education, Science and Culture of Japan, a Grant-in-Aid for Cancer Research from the Ministry of Health, Labour and Welfare of Japan (13-2), and the Uehara Memorial Foundation.

Appendix A. Supplementary data

Supplementary data associated with this article can be found, in the online version, at doi:10.1016/j.ydbio.2010.07.015.

References

Audigier, S., Guiramand, J., Prado-Lourenco, L., Conte, C., Gonzalez-Herrera, I.G., Cohen-Solal, C., Récasens, M., Prats, A.C., 2008. Potent activation of FGF-2 IRES-dependent mechanism of translation during brain development. RNA 14, 1852–1864.

Bee, T., Swiers, G., Muroi, S., Pozner, A., Nottingham, W., Santos, A.C., Li, P.S., Taniuchi, I., de Bruijn, M.F., 2010. Nonredundant roles for Runx1 alternative promoters reflect their activity at discrete stages of developmental hematopoiesis. Blood 115, 3042–3050.

Blyth, K., Cameron, E.R., Neil, J.C., 2005. The RUNX genes: gain or loss of function in cancer. Nat. Rev. Cancer 5, 376–387.

Davis, S., Aldrich, T.H., Jones, P.F., Acheson, A., Compton, D.L., Jain, V., Ryan, T.E., Bruno, J., Radziejewski, C., Maisonpierre, P.C., Yancopoulos, G.D., 1996. Isolation of angiopoietin-1, a ligand for the TIE2 receptor, by secretion-trap expression cloning. Cell 87, 1161–1169.

Dobbyn, H.C., Hill, K., T.L.H., Spriggs, K.A., Pickering, B.M., Coldwell, M.J., de Moor, C.H., Bushell, M., Willis, A.E., 2008. Regulation of BAG-1 IRES-mediated translation following chemotoxic stress. Oncogene 27, 1167–1174.

Downing, J.R., 2003. The core-binding factor leukemias: lessons learned from murine models. Curr. Opin. Genet. Dev. 13, 48–54.

Ema, H., Morita, Y., Nakauchi, H., Matsuzaki, Y., 2005. Isolation of murine hematopoietic stem cells and progenitor cells. Curr. Protoc. Immunol. Chapter 22, Unit 22B.1. Supplement 67.

Ghozi, M.C., Bernstein, Y., Negreanu, V., Levanon, D., Groner, Y., 1996. Expression of the human acute myeloid leukemia gene AML1 is regulated by two promoter regions. Proc. Natl. Acad. Sci. U. S. A. 93, 1935–1940.

Gonzalez-Herrera, I.G., Prado-Lourenco, L., Pileur, F., Conte, C., Morin, A., Cabon, F., Prats, H., Vagner, S., Bayard, F., Audigier, S., Prats, A.C., 2006. Testosterone regulates FGF-2 expression during testis maturation by an IRES-dependent translational mechanism. FASEB J. 20, 476–478.

Growney, J.D., Shigematsu, H., Li, Z., Lee, B.H., J.A., Rowan, R., Curley, D.P., Kutok, J.L., Akashi, K., Williams, I.R., Speck, N.A., Gilliland, D.G., 2005. Loss of Runx1 perturbs adult hematopoiesis and is associated with a myeloproliferative phenotype. Blood 106, 494–504.

Holcik, M., Sonenberg, N., 2005. Translational control in stress and apoptosis. Nat. Rev. Mol. Cell Biol. 6, 318–327.

Honda, H., Oda, H., Nakamoto, T., Honda, Z., Sakai, R., Suzuki, T., Saito, T., Nakamura, K., Nakao, K., Ishikawa, T., Katsuki, M., Yazaki, Y., Hirai, H., 1998. Cardiovascular anomaly, impaired actin bundling and resistance to Src-induced transformation in mice lacking p130Cas. Nat. Genet. 19, 361–365.

Ichikawa, M., Asai, T., Saito, T., Seo, S., Yamazaki, I., Yamagata, T., Mitani, K., Chiba, S., Ogawa, S., Kurokawa, M., Hirai, H., 2004. AML-1 is required for megakaryocytic maturation and lymphocytic differentiation, but not for maintenance of hematopoietic stem cells in adult hematopoiesis. Nat. Med. 10, 299–304.

Jo, O.D., Martin, J., Bernath, A., Masri, J., Lichtenstein, A., Gera, J., 2008. Heterogeneous nuclear ribonucleoprotein A1 regulates cyclin D1 and c-myc internal ribosome entry site function through Akt signaling. J. Biol. Chem. 283, 23274–23287.

Kubo, H., Alitalo, K., 2003. The bloody fate of endothelial stem cells. Genes Dev. 17, 322–329.

Lacaud, G., Gore, L., Kennedy, M., Kouskoff, V., Kingsley, P., Hogan, C., Carlsson, L., Speck, N., Palis, J., Keller, G., 2002. Runx1 is essential for hematopoietic commitment at the hemangioblast stage of development in vitro. Blood 100, 458–466.

Levanon, D., Groner, Y., 2004. Structure and regulated expression of mammalian RUNX genes. Oncogene 23, 4211–4219.

Levanon, D., Glusman, G., Bangsow, T., Ben-Asher, E., Male, D.A., Avidan, N., Bangsow, C., Hattori, M., Taylor, T.D., Taudien, S., Blechschmidt, K., Shimizu, N., Rosenthal, A., Sakaki, Y., Lancet, D., Groner, Y., 2001. Architecture and anatomy of the genomic locus encoding the human leukemia-associated transcription factor RUNX1/AML1. Gene 262, 23–33.

Ma, F., Wada, M., Yoshino, H., Ebihara, Y., Ishii, T., Manabe, A., Tanaka, R., Maekawa, T., Ito, M., Mugishima, H., Asano, S., Nakahata, T., Tsuji, K., 2001. Development of human lymphohematopoietic stem and progenitor cells defined by expression of CD34 and CD81. Blood 97, 3755–3762.

Maki, K., Yamagata, T., Asai, T., Yamazaki, I., Oda, H., Hirai, H., Mitani, K., 2005. Dysplastic definitive hematopoiesis in AML1/EVI1 knock-in embryos. Blood 106, 2147–2155.

Maki, K., Yamagata, T., Yamazaki, I., Oda, H., Mitani, K., 2006. Development of megakaryoblastic leukaemia in Runx1-Evi1 knock-in chimaeric mouse. Leukemia 20, 1458–1460.

Meijer, H.A., Thomas, A.A., 2002. Control of eukaryotic protein synthesis by upstream open reading frames in the 5′-untranslated region of an mRNA. Biochem. J. 367, 1.

Meuer, H.J., Hartmann, V., Jopp, S., 1992. Tissue PO2 and growth rate in early chick embryos. Respir. Physiol. 90, 227–237.

Mikhail, F.M., Sinha, K.K., Saunthararajah, Y., Nucifora, G., 2006. Normal and transforming functions of RUNX1: a perspective. J. Cell. Physiol. 207, 582–593.

Mitani, K., Ogawa, S., Tanaka, T., Miyoshi, H., Kurokawa, M., Mano, H., Yazaki, Y., Ohki, M., Hirai, H., 1994. Generation of the AML1-EVI-1 fusion gene in the t(3;21)(q26;q22) causes blastic crisis in chronic myelocytic leukemia. EMBO J. 13, 504–510.

Mitchell, S.A., Spriggs, K.A., Coldwell, M.J., Jackson, R.J., Willis, A.E., 2003. The Apaf-1 internal ribosome entry segment attains the correct structural conformation for function via interactions with PTB and unr. Mol. Cell 11, 757–771.

Miyazaki, K., Kawamoto, T., Tanimoto, K., Nishiyama, M., Honda, H., Kato, Y., 2002. Identification of functional hypoxia response elements in the promoter region of the DEC1 and DEC2 genes. J. Biol. Chem. 277, 47014–47021.

Morita, Y., Ema, H., Yamazaki, S., Nakauchi, H., 2006. Non-side-population hematopoietic stem cells in mouse bone marrow. Blood 108, 2850–2856.

Nakahata, T., Ogawa, M., 1982. Hemopoietic colony-forming cells in umbilical cord blood with extensive capability to generate mono- and multipotential hemopoietic progenitors. J. Clin. Invest. 70, 1324–1328.

Okada, H., Watanabe, T., Niki, M., Takano, H., Chiba, N., Yanai, N., Tani, K., Hibino, H., Asano, S., Mucenski, M.L., Ito, Y., Noda, T., Satake, M., 1998. AML1(−/−) embryos do not express certain hematopoiesis-related gene transcripts including those of the PU.1 gene. Oncogene 17, 2287–2293.

Okuda, T., van Deursen, J., Hiebert, S.W., Grosveld, G., Downing, J.R., 1996. AML1, the target of multiple chromosomal translocations in human leukemia, is essential for normal fetal liver hematopoiesis. Cell 84, 321–330.

Okuda, T., Takeda, K., Fujita, Y., Nishimura, M., Yagyu, S., Yoshida, M., Akira, S., Downing, J.R., Abe, T., 2000. Biological characteristics of the leukemia-associated transcriptional factor AML1 disclosed by hematopoietic rescue of AML1-deficient embryonic stem cells by using a knock-in strategy. Mol. Cell. Biol. 20, 319–328.

Osato, M., 2004. Point mutations in the RUNX1/AML1 gene: another actor in RUNX leukemia. Oncogene 23, 4284–4296.

Pickering, B.M., Willis, A.E., 2005. The implications of structured 5′ untranslated regions on translation and disease. Semin. Cell Dev. Biol. 16, 39–47.

Pozner, A., Goldenberg, D., Negreanu, V., Le, S.Y., Elroy-Stein, O., Levanon, D., Groner, Y., 2000. Transcription-coupled translation control of AML1/RUNX1 is mediated by cap- and internal ribosome entry site-dependent mechanisms. Mol. Cell. Biol. 20, 2297–2307.

Pozner, A., Lotem, J., Xiao, C., Goldenberg, D., Brenner, O., Negreanu, V., Levanon, D., Groner, Y., 2007. Developmentally regulated promoter-switch transcriptionally controls Runx1 function during embryonic hematopoiesis. BMC Dev. Biol. 7, 1–19.

Putz, G., Rosner, A., Nuesslein, I., Schmitz, N., Buchholz, F., 2006. AML1 deletion in adult mice causes splenomegaly and lymphomas. Oncogene 25, 929–939.

Song, W.J., Sullivan, M.G., Legare, R.D., Hutchings, S., Tan, X., Kufrin, D., Ratajczak, J., Resende, I.C., Haworth, C., Hock, R., Loh, M., Felix, C., Roy, D.C., Busque, L., Kurnit, D., Willman, C., Gewirtz, A.M., Speck, N.A., Bushweller, J.H., Li, F.P., Gardiner, K., Poncz, M., Maris, J.M., Gilliland, D.G., 1999. Haploinsufficiency of CBFA2 causes familial thrombocytopenia with propensity to develop acute myelogenous leukaemia. Nat. Genet. 23, 166–175.

Spriggs, K.A., Stoneley, M., Bushell, M., Willis, A.E., 2008. Re-programming of translation following cell stress allows IRES-mediated translation to predominate. Biol. Cell 100, 27–38.

Stoneley, M., Willis, A.E., 2004. Cellular internal ribosome entry segments: structures, trans-acting factors and regulation of gene expression. Oncogene 23, 3200–3207.

Suda, T., Takakura, N., 2001. Role of hematopoietic stem cells in angiogenesis. Int. J. Hematol. 74, 266–271.

Takakura, N., Watanabe, T., Suenobu, S., Yamada, Y., Noda, T., Ito, Y., Satake, M., Suda, T., 2000. A role for hematopoietic stem cells in promoting angiogenesis. Cell 102, 199–209.

Wang, Q., Stacy, T., Binder, M., Marin-Padilla, M., Sharpe, A.H., Speck, N.A., 1996. Disruption of the Cbfa2 gene causes necrosis and hemorrhaging in the central nervous system and blocks definitive hematopoiesis. Proc. Natl. Acad. Sci. U. S. A. 93, 3444–3449.

THE JOURNAL OF BIOLOGICAL CHEMISTRY VOL. 285, NO. 3, pp. 1850–1860, January 15, 2010

Up-regulation of Survivin by the E2A-HLF Chimera Is Indispensable for the Survival of t(17;19)-positive Leukemia Cells*

Received for publication, June 10, 2009, and in revised form, October 29, 2009 Published, JBC Papers in Press, November 2, 2009, DOI 10.1074/jbc.M109.023762

Mayuko Okuya[‡], Hidemitsu Kurosawa[‡1], Jiro Kikuchi[§], Yusuke Furukawa[§], Hirotaka Matsui[¶], Daisuke Aki[¶], Takayuki Matsunaga[‡], Takeshi Inukai[‖], Hiroaki Goto[**], Rachel A. Altura[‡‡], Kenich Sugita[‡], Osamu Arisaka[‡], A. Thomas Look[§§], and Toshiya Inaba[¶]

From the [‡]Department of Pediatrics, Dokkyo Medical University School of Medicine, Tochigi 321-0293, Japan, the [§]Division of Stem Cell Regulation Center for Molecular Medicine, Jichi Medical School, Tochigi 329-0498, Japan, the [¶]Department of Molecular Oncology, Research Institute for Radiation Biology and Medicine, Hiroshima University, Hiroshima 734-8553, Japan, the [‖]Department of Pediatrics, University of Yamanashi School of Medicine, Yamanashi 409-3898, Japan, the [**]Department of Pediatrics, Yokohama City University School of Medicine, Kanagawa 236-0004, Japan, the [‡‡]Department of Pediatrics, The Warren Alpert Medical School of Brown University, Providence, Rhode Island 02903, and the [§§]Pediatric Oncology Department, Dana-Farber Cancer Institute, Boston, Massachusetts 02115

The E2A-HLF fusion transcription factor generated by t(17;19)(q22;p13) translocation is found in a small subset of pro-B cell acute lymphoblastic leukemias (ALLs) and promotes leukemogenesis by substituting for the antiapoptotic function of cytokines. Here we show that t(17;19)$^+$ ALL cells express Survivin at high levels and that a dominant negative mutant of E2A-HLF suppresses Survivin expression. Forced expression of E2A-HLF in t(17;19)$^-$ leukemia cells up-regulated Survivin expression, suggesting that Survivin is a downstream target of E2A-HLF. Analysis using a counterflow centrifugal elutriator revealed that t(17;19)$^+$ ALL cells express Survivin throughout the cell cycle. Reporter assays revealed that E2A-HLF induces *survivin* expression at the transcriptional level likely through indirect down-regulation of a cell cycle-dependent *cis* element in the promoter region. Down-regulation of Survivin function by a dominant negative mutant of Survivin or reduction of Survivin expression induced massive apoptosis throughout the cell cycle in t(17;19)$^+$ cells mainly through caspase-independent pathways involving translocation of apoptosis-inducing factor (AIF) from mitochondria to the nucleus. AIF knockdown conferred resistance to apoptosis caused by down-regulation of Survivin function. These data indicated that reversal of AIF translocation by Survivin, which is induced by E2A-HLF throughout the cell cycle, is one of the key mechanisms in the protection of t(17;19)$^+$ leukemia cells from apoptosis.

The E2A-HLF fusion transcription factor, which is generated by the t(17;19)(q22;p13) translocation, is found in a small subset of pro-B cell acute lymphoblastic leukemias (ALLs)[2] that occurs in older children and adolescents (1, 2). In this chimeric molecule, the *trans*-activation domain of E2A is fused to the basic region and leucine zipper domain of HLF, which mediates DNA binding and dimerization. Patients with this chimera share distinct clinical features such as hypercalcemia and coagulopathy and very poor prognosis because of resistance to intensive chemotherapy, including aggressive conditioning for bone marrow transplantation (3–5), all of which are unusual for pro-B cell ALLs. Thus, these features may be a direct consequence of aberrant gene expression induced by E2A-HLF fusion transcription factor, rather than a consequence of the nature of B cell progenitors.

We previously demonstrated that inhibition of the *trans*-activation potential of the E2A-HLF chimera by a dominant negative mutant results in apoptosis in t(17;19)$^+$ ALL cells but does not affect the cell cycle (6). Moreover, E2A-HLF blocks apoptosis normally induced by cytokine deprivation in murine interleukin (IL)-3-dependent B precursor lines such as Baf-3 or FL5.12 cells, suggesting that this fusion protein contributes to leukemogenesis through modification of apoptosis regulatory pathways normally controlled by cytokines (6, 7). We speculated that the target genes of E2A-HLF involved in the inhibition of apoptosis are those regulated via Ras pathways in IL-3-dependent cells, because activation of Ras pathways is indispensable for long term survival of Baf-3 cells in cytokine-free medium (8, 9). Moreover, we previously identified E4BP4/NFIL3, a related basic region and leucine zipper factor with antiapoptotic function, as a possible physiological counterpart of E2A-HLF (10), and we found that E4BP4 expression is induced by IL-3 through Ras-phosphatidylinositol 3-kinase and Ras-Raf-MAPK pathways in IL-3-dependent cells (9).

The *survivin* gene may be a good candidate for a target gene of E2A-HLF involved in the inhibition of apoptosis in t(17;19)$^+$

* This work was supported by Grant-in-aid for Scientific Research (C) 18591201 from the Japan Society for Promotion of Science (to H. K.) and a young investigator award from Dokkyo Medical University (to M. O.).

[1] To whom correspondence should be addressed: Dept. of Pediatrics, Dokkyo Medical University, Mibu, Tochigi 321-0293, Japan. Tel.: 81-282-86-1111; Fax: 81-282-86-2947; E-mail: hidekuro@dokkyomed.ac.jp.

[2] The abbreviations used are: ALL, acute lymphoblastic leukemia; AIF, apoptosis-inducing factor; IL, interleukin; MAPK, mitogen-activated protein kinase; CHR, cell cycle homology region; PBS, phosphate-buffered saline; FITC, fluorescein isothiocyanate; shRNA, short hairpin RNA; siRNA, short interfering RNA; GFP, green fluorescent protein; EMSA, electrophoretic mobility shift assay; BrdUrd, bromodeoxyuridine; TdT, terminal deoxynucleotidyltransferase; PARP, poly(ADP-ribose) polymerase; TUNEL, terminal deoxynucleotidyltransferase-mediated dUTP nick-end-labeling; PI, propidium iodide; dn, dominant negative; nt, nucleotide; 7-AAD, 7-amino-actinomycin D; PLL, plenti-Lox3.7.

ALL cells. Survivin, at 142 amino acids, is the smallest member of the inhibitor of apoptosis protein family and significantly prolongs the viability of cytokine-deprived IL-3-dependent cells (11). The expression of Survivin is controlled by oncogenic c-H-ras, and up-regulation of Survivin depends on functional Ras/phosphatidylinositol 3-kinase and Ras-Raf-MAPK signaling pathways (12). Overexpression of Survivin can protect cells from both extrinsically and intrinsically induced apoptosis (13, 14), whereas inhibition of Survivin expression by antisense ribozyme or RNA interference leads to increased spontaneous apoptosis (15, 16).

A unique feature of Survivin as an apoptosis regulator is its involvement in cell cycle progression (17). *survivin* expression is transcriptionally induced in the G_2/M phase through cell cycle-dependent *cis* elements located near the transcription initiation site (16). These elements, including the cell cycle-dependent element (GGCGG) and the cell cycle homology region (CHR; ATTTGAA), are implicated in G_1 transcriptional repression in S/G_2-regulated genes, such as cyclin A, cdc25C, and cdc2 (18). In addition, Survivin is activated through phosphorylation of Thr-34 by mitotic kinase CDC2-cyclin-B1 (14). Enforced expression of a phosphorylation-defective Survivin T34A mutant (Survivin-T34A) initiates mitochondrial dependent apoptosis in a variety of tumor cell lines (14, 16).

Here, we show that Survivin expression is induced by the E2A-HLF chimera, and down-regulation of Survivin induces caspase-independent massive apoptosis in t(17;19)$^+$ ALL cell lines. These findings indicate that Survivin contributes to leukemogenesis by subverting genetic pathways responsible for the apoptosis of B cell progenitors.

EXPERIMENTAL PROCEDURES

Cell Lines and Cell Culture—Human ALL cell lines that express E2A-HLF (UOC-B1, HAL-O1, YCUB-2, and Endo-kun) and other leukemia cell lines (Nalm-6, RS4;11, REH, 697, 920, HL-60, NB-4, and Jurkat) were cultured in RPMI 1640 medium containing 10% fetal bovine serum. Establishment of Nalm-6 human pro-B cell leukemia cells that express zinc-inducible E2A-HLF (Nalm-6/E2A-HLF) using the pMT-CB6$^+$ eukaryotic expression vector (a gift from Dr. F. Rauscher III, Wistar Institute, Philadelphia) has been described previously (19). UOC-B1/E2A-HLF(dn) cells transfected with a dominant negative mutant of E2A-HLF, which lacks the AD1 transactivation domain of E2A and contains a mutated HLF DNA-binding domain with an intact leucine-zipper domain, were prepared as described previously (6). UOC-B1, Endo-kun, REH, and Jurkat cells that were transfected with either the pMT/Survivin-T34A vector or the empty pMT-CB6$^+$ vector were designated as UOC-B1/Survivin(dn), UOC-B1/pMT, Endo-kun/Survivin(dn), Endo-kun/pMT, REH/Survivin(dn), REH/pMT, Jurkat/Survivin(dn), and Jurkat/pMT, respectively.

Counterflow Centrifugal Elutriations—Counterflow centrifugal elutriations were performed using the SRR6Y elutriation system and rotor equipped with a 4.5-ml chamber (Hitachi Koki Co., Ltd., Tokyo, Japan) (20). Target cells were resuspended at 1–2 × 10^8 cells in 50 ml of PBS containing 1% fetal bovine serum and injected into the elutriation system at 4 °C using an initial flow rate of 16 ml/min and rotor speed of 2,000 rpm. The flow rate was incrementally increased, and cell fractions were collected serially as follows: fraction 1, 200 ml at 16 ml/min; fraction 2, 200 ml at 18 ml/min; fraction 3, 200 ml at 20 ml/min; fraction 4, 200 ml at 22 ml/min; fraction 5, 200 ml at 24 ml/min; fraction 6, 200 ml at 26 ml/min; and fraction 7, 200 ml at 28 ml/min. Cell cycle analysis was performed on each fraction by staining DNA with propidium iodide (PI) in preparation for flow cytometry with the FACScan/CellFIT system (BD Biosciences).

Gene Silencing by RNA Interference—Short hairpin/short interfering RNA (shRNA/siRNA) was introduced into UOC-B1 or UOC-B1/Survivin(dn) cells to down-regulate the expression of Survivin or apoptosis-inducing factor (AIF) by the shRNA lentivirus system (21, 22). Oligonucleotides were chemically synthesized, annealed, terminally phosphorylated, and inserted into the vector pLL3.7 (Addgene, Cambridge, MA). Oligonucleotides containing siRNA target for *survivin* sequences (23) were as follows: 5′-TGAAGCGTCTGGCAGATACTTTCAAGAGAAGTATCTGCCAGACGCTTCTTTTTTC-3′ (forward 1) and 5′-TCGAGAAAAAAGAAGCGTCTGGCAGATACTTCTCTTGAAAGTATCTGCCAGACGTTCA-3′ (reverse 1); 5′-TGTGGATGAGGAGACAGAATTTCAAGAGAATTCTGTCTCCTCATCCACTTTTTTC-3′ (forward 3) and 5′-TCGAGAAAAAAGTGGATGAGGAGACAGAATTCTCTTGAAATTCTGTCTCCTCATCCACA-3′ (reverse 3); 5′-TGGATACTTCACTTTAATAATTCAAGAGATTATTAAAGTGAAGTATCCTTTTTTC-3′ (forward 4) and 5′-TCGAGAAAAAAGGATACTTCACTTTAATAATCTCTTGAATTATTAAAGTGAAGTATCCA-3′ (reverse 4); 5′-TGCTTCCTCGACATCTGTTATTCAAGAGATAACAGATGTCGAGGAAGCTTTTTTC-3′ (forward 5) and 5′-TCGAGAAAAAAGCTTCCTCGACATCTGTTATCTCTTGAATAACAGATGTCGAGGAAGCA-3′ (reverse 5). Oligonucleotides containing siRNA target for *AIF* sequences were as follows: 5′-TGGAGGAGTCTGCGTAATGTTTCAAGAGAACATTACGCAGACTCCTCCTTTTTTC-3′ (forward 1) and 5′-TCGAGAAAAAAGGAGGAGTCTGCGTAATGTTCTCTTGAAACATTACGCAGACTCCTCCT-3′ (reverse 1); 5′-TGCAGGAAGGTAGAAACTGATTCAAGAGATCAGTTTCTACCTTCCTGCTTTTTTC-3′ (forward 2) and 5′-TCGAGAAAAAAGCAGGAAGGTAGAAACTGATCTCTTGAATCAGTTTCTACCTTCCTGCT-3′ (reverse 2); 5′-TGCATGCTTCTACGATATAATTCAAGAGATTATATCGTAGAAGCATGCTTTTTTC-3′ (forward 3) and 5′-TCGAGAAAAAAGCATGCTTCTACGATATAATCTCTTGAATTATATCGTAGAAGCATGCT-3′ (reverse 3); the nucleotide sequences corresponding to the siRNA are underlined. The resulting plasmids or the parental pLL3.7, along with lentiviral packaging mix (ViraPower, Invitrogen), was transfected into 293FT cells (Invitrogen) to produce recombinant lentivirus, and the UOC-B1 or UOC-B1/Survivin(dn) cells were infected with the virus. Enhanced green fluorescent protein (GFP)-positive cells were purified by FACSAria (BD Biosciences) as shRNA-transfected cell populations.

Reporter Assay—Fragments of the 5′-flanking region of the human *survivin* gene spanning 147, 213, 288, 503, or 698 bp were generated by PCR using *Pfu* polymerase from genomic DNA of human placenta. The positions of the forward (5′)

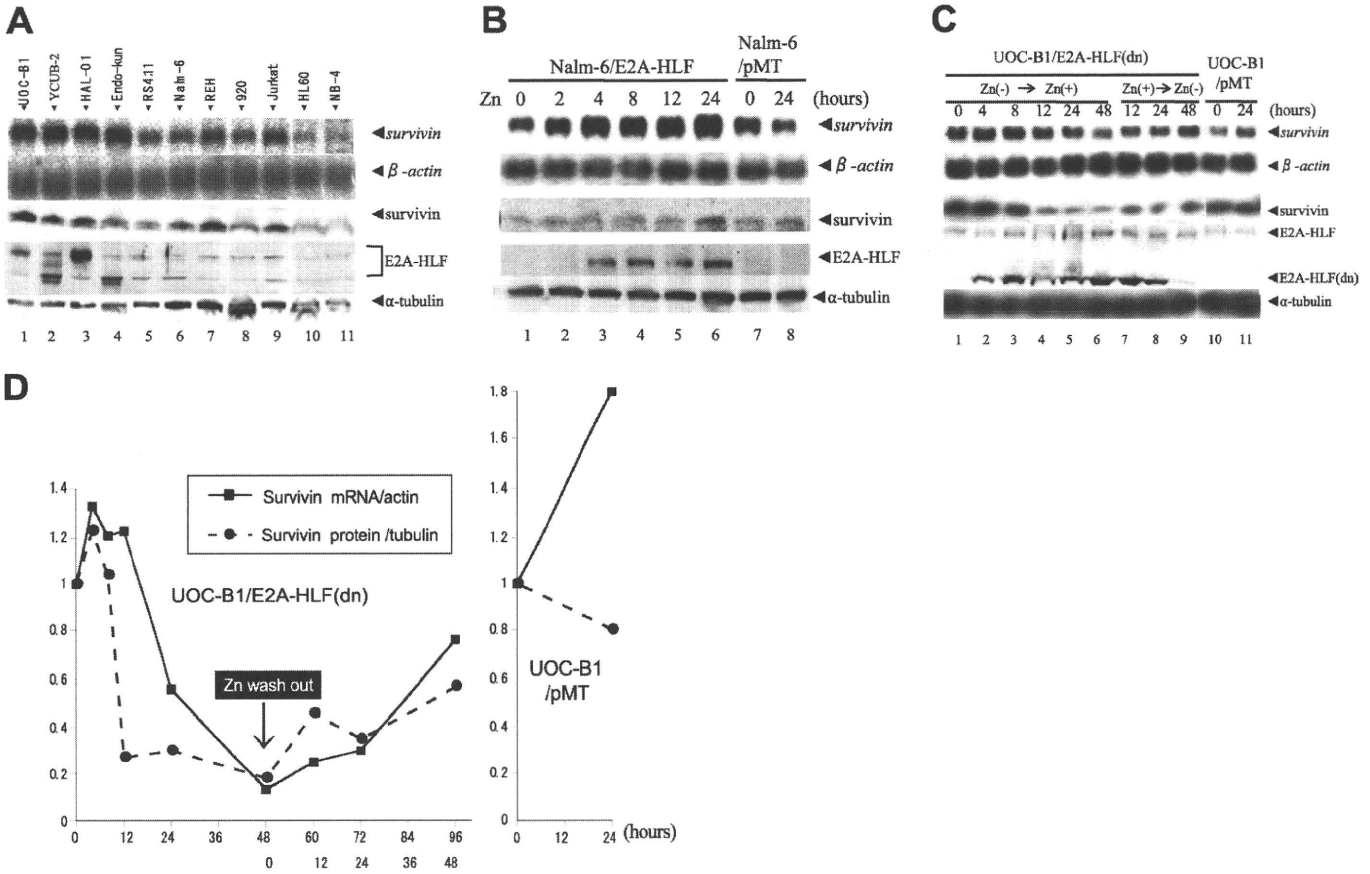

FIGURE 1. **Expression of Survivin in human leukemia cell lines and induction of Survivin by E2A-HLF in human ALL cells.** *A, top 2 panels,* Northern blot analysis of poly(A)$^+$ RNA isolated from human leukemia cell lines. The blot was hybridized with a *survivin* cDNA probe and then rehybridized with a β-actin probe. *Lower three panels,* immunoblot analysis using whole-cell lysates. Survivin, E2A-HLF, and α-tubulin proteins were detected with specific antibodies. *Lanes 1–4,* the UOC-B1, YCUB-2, HAL-O1, and Endo-kun t(17;19)-positive pro-B ALL cell lines; *lanes 5–8,* the RS4;11, Nalm-6, REH, and 920 pro-B ALL cell lines without t(17;19); *lane 9,* the Jurkat T-ALL cell line; *lane 10,* the HL-60 AML cell line; and *lane 11,* the NB-4 APL cell line. *B,* Nalm-6 cells with zinc-inducible expression of E2A-HLF (Nalm-6/E2A-HLF) and control Nalm-6/pMT cells were cultured in medium containing 100 μM zinc for the indicated length of time. *C* and *D,* UOC-B1 cells with zinc-inducible expression of E2A-HLF(dn) (UOC-B1/E2A-HLF(dn)) and control UOC-B1/pMT cells were cultured in medium containing 100 μM zinc for the indicated length of time (*Zn*(−) → *Zn*(+)) and removal of zinc from the growth medium (*Zn*(+) → *Zn*(−)). *C, upper two panels,* Northern blot analysis of poly(A)$^+$ RNA. The blot was hybridized with a *survivin* cDNA probe and then rehybridized with a β-actin probe. *Lower three panels,* immunoblot analysis for Survivin, E2A-HLF, or α-tubulin proteins. *D,* quantification of intensity of each band.

primers with respect to the translational initiation codon (according to NCBI GenBank™ sequence U75285) are −124 (−124 forward primer, 5′-ACTCCCAGAAGGCCGCGGGGGGTG-3′), −190 (5′-ACCACGGGCAGAGCCACGCGGCGGG-3′), −265 (5′-GTTCTTTGAAAGCAGTCGAGGGGGC-3′), −480 (5′-CGGGTTGAAGCGATTCTCCTGCCT-3′), and −675 (5′-CGATGTCTGCACTCCATCCCTC-3′). The reverse (3′) primer used for these amplifications was at position 23 (+23-reverse primer, 5′-GGGGGCAACGTCGGGGCAagCtTGC-3′) and was constructed based on the genomic sequence with a modification (lowercase) to create a HindIII site. The PCR products were cloned into a pGL3-basic vector (Promega, Madison, WI). The resulting reporter plasmids were designated as pGL3-124, pGL3-190, pGL3-265, pGL3-480, and pGL3-675, respectively. The pGL3-124mut1 vector containing two mutated cell cycle-dependent elements (−6 and −12) was generated by PCR using the −124 forward primer and a reverse primer (5′-GCAAGCTTGtcactGtcactACCTCTG-3′); pGL3-124mut2 vector containing mutated CHR (−42) in addition to two mutated cell cycle-dependent elements (−6 and −12) was generated by the −124 forward primer and a reverse primer (5′-GCAAGCTTGtcactGtcactACCTCTGCCAACGGGTCCCGCGATTCgggTCTGG-3′); and pGL3-124mut3 vector containing a mutated CHR (−42) was generated by the −124 forward primer and a reverse primer (5′-GCAAGCTTGCCGCCGCCGCCACCTCTGCCAACGGGTCCCGCGATTCgggTCTGG-3′) (lowercase indicates mutations).

For transfection with a pMT-CB6$^+$/E2A-HLF construct, Nalm-6 cells (6×10^4) were seeded into 24-well plates, cotransfected with pGL3-*survivin* promoter construct plus pRL-TK vector, which contains the *Renilla* luciferase gene, by Lipofectamine 2000 (Invitrogen), and harvested 24 h later. E2A-HLF expression was induced in Nalm-6 cells by the addition of 100 μM $ZnCl_2$ 24 h after transfection. Firefly luciferase and *Renilla* luciferase as a transfection efficiency control were detected with Dual-Luciferase Reporter Assay System (Promega) according to the manufacturer's instructions and measured in a Veritas Microplate Luminometer (Promega).

Electrophoretic Mobility Shift Assays (EMSA)—EMSA were performed by incubating 12 μg of nuclear protein lysate at 30 °C for 15 min with a ^{32}P-end-labeled DNA oligonucleotide probe (2×10^4 cpm) containing the CHR-binding site sequence

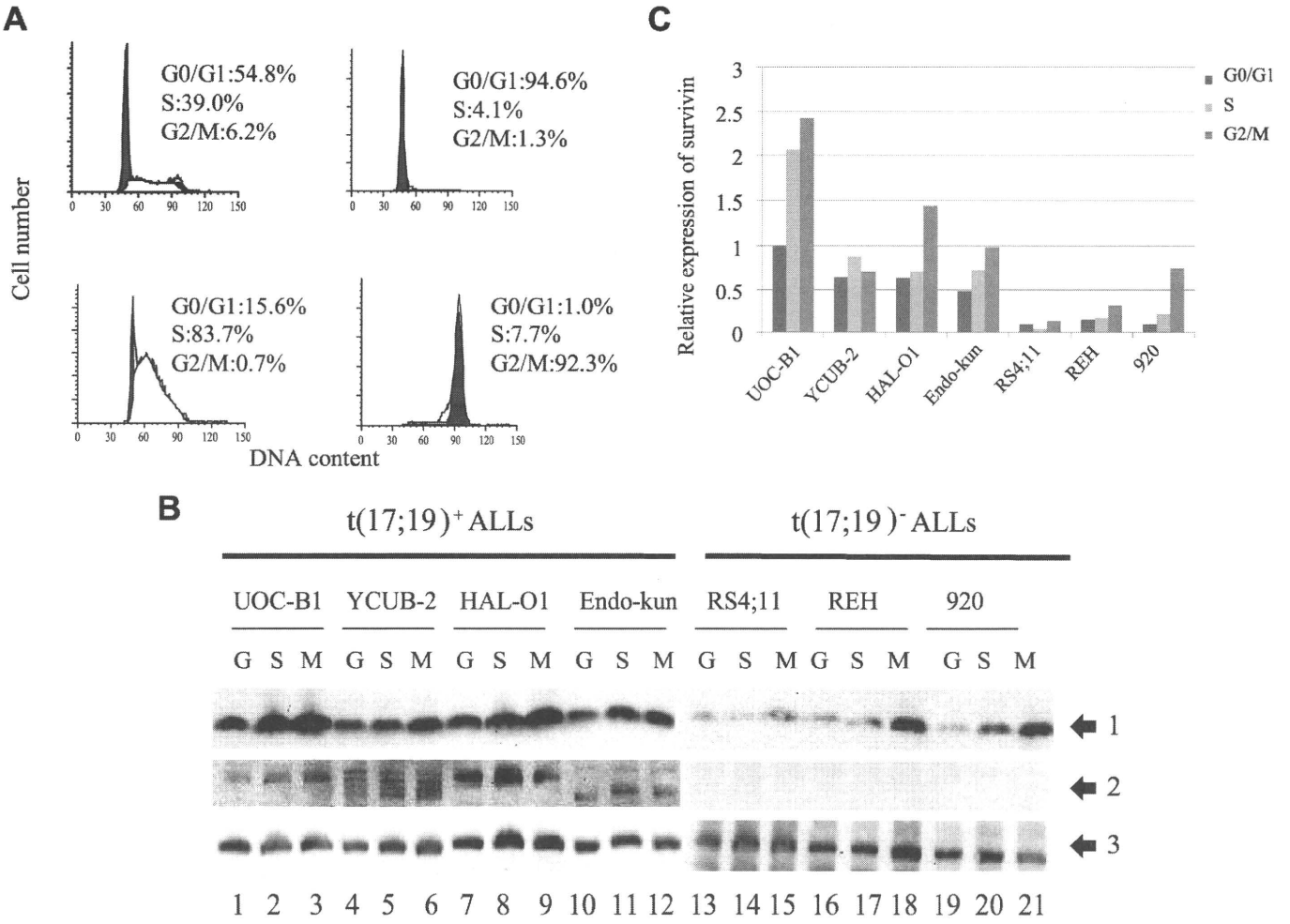

FIGURE 2. **Cell cycle-dependent and -independent expression of Survivin in human leukemia cells.** Fractions enriched with cells at each phase of the cell cycle were separated by counterflow centrifugal elutriation. *A,* representative DNA histogram of each fraction subjected to flow cytometry after staining DNA with PI. *Upper left,* no fractionation; *upper right,* G_0/G_1 phase-enriched fraction; *lower left,* S-phase-enriched fraction; *lower right,* G_2/M-phase-enriched fraction. *B,* immunoblot analysis of fractions of $t(17;19)^+$ ALL cells or $t(17;19)^-$ ALL cells enriched with cells in the G_0/G_1- (*G*), S- (*S*), or G_2/M (*M*)-phase. Survivin (*arrow 1*), E2A-HLF (*arrow 2*), and α-tubulin (*arrow 3*) proteins were detected with specific antibodies. *C,* levels of Survivin and α-tubulin proteins were determined by the band intensity on autoradiograms from *B*. Levels of Survivin were normalized to levels of α-tubulin, and amounts shown are relative to amounts in UOC-B1 cells in the G_0/G_1-phase.

in the *survivin* promoter (5′-CATTAACCGCCAGATTTGAATCGCGG-3′) in a solution of 12% glycerol, 12 mM HEPES (pH 7.9), 4 mM Tris (pH 7.9), 133 mM KCl, 1.5 μg of sheared calf thymus DNA, and 300 μg of bovine serum albumin per ml as described previously (24). In the competitive inhibition experiments, excess of the unlabeled CHR-consensus sequence probe, *i.e.* oligonucleotide containing the candidate-binding sites of CHR in the *survivin* gene promoter or its 3-bp mismatched oligonucleotide (5′-CATTAACCGCCAGAcccGAATCGCGG-3′) was added to the reaction mixture. The entire mixture was incubated at 30 °C for 15 min. Nondenaturing polyacrylamide gels containing 4% acrylamide and 2.5% glycerol were prerun at 4 °C in a high ionic strength Tris-glycine buffer for 30 min and run at 50 mA for ~45 min. The gel was then dried under vacuum and analyzed by autoradiography.

Other Experimental Procedures—For visualization of intracellular AIF, cytospinned cells were fixed with 1% paraformaldehyde in PBS for 10 min, and permeabilized with 0.5% Triton X-100 in PBS for 5 min. Cells were rinsed twice with PBS (5 min for each rinse), blocked with 5% goat serum in PBS for 30 min, and incubated with anti-AIF antibody (1:100; Santa Cruz Biotechnology, Santa Cruz, CA) overnight at 4 °C in a humidified chamber. Cells were incubated with a secondary antibody, fluorescein isothiocyanate (FITC)-labeled anti-goat IgG (1:500; Santa Cruz Biotechnology), at 37 °C for 30 min.

For Northern blot analysis, 1 μg of poly(A)-selected RNA was separated by electrophoresis in 1% agarose gels containing 2.2 M formaldehyde, transferred to nylon membranes, and hybridized with the appropriate probe according to standard procedures as described previously (5). For immunoblot analysis, the primary antibodies used were anti-Survivin polyclonal (R & D Systems, Minneapolis, MN), anti-α-tubulin monoclonal (Sigma), anti-caspase 3 polyclonal (Cell Signaling Technology, Beverly, MA), anti-caspase 9 polyclonal (BD Biosciences), anti-PARP monoclonal (BD Biosciences), and anti-AIF polyclonal antibodies (Santa Cruz Biotechnology). Anti-HLF(C) antibody for detection of the E2A-HLF chimeric protein was described previously (24).

Cell viability was determined by trypan blue dye exclusion. Early apoptotic events were detected by flow cytometric mea-

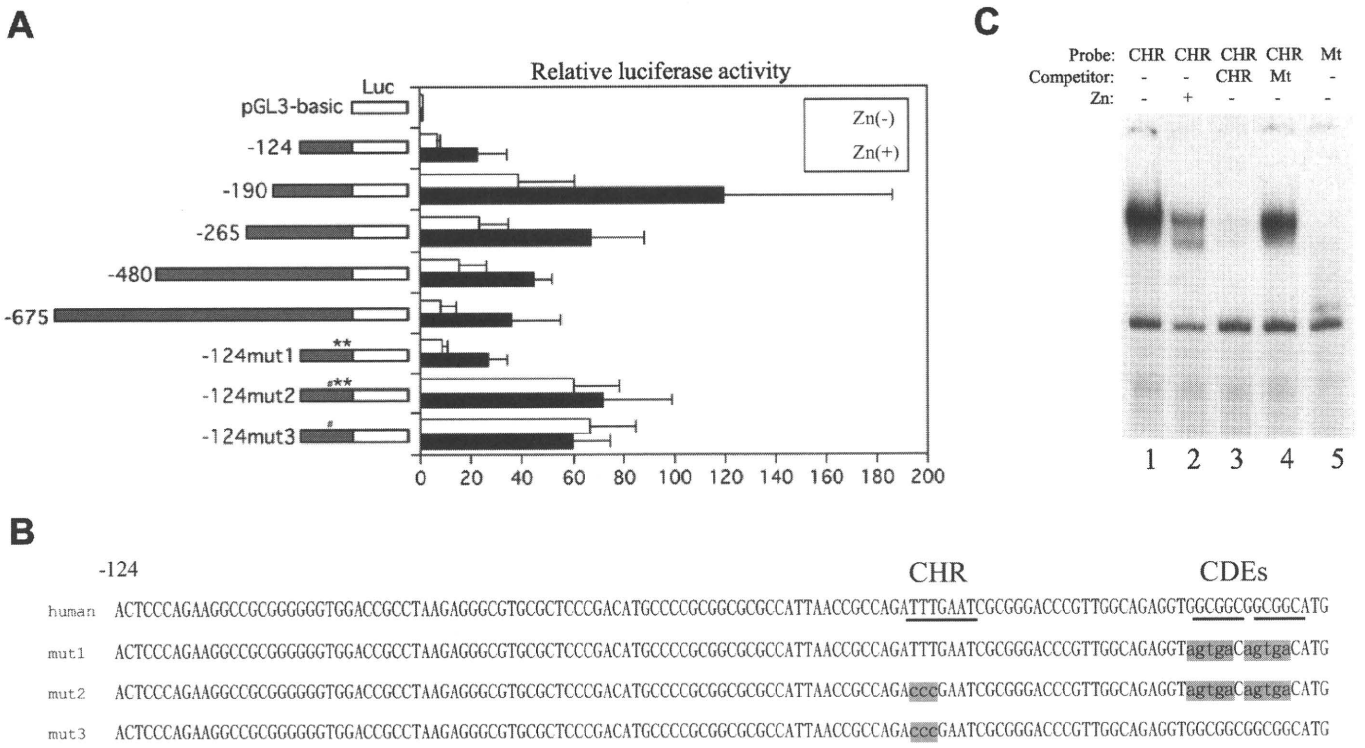

FIGURE 3. **Effect of E2A-HLF on *survivin* promoter activity in transiently transfected t(17;19)$^-$ ALL cells.** *A*, Nalm-6/E2A-HLF cells cotransfected with pRL-TK vector and the pGL3-*survivin* promoter constructs indicated at the *left* were cultured in the absence (*open bars*) or presence (*black bars*) of zinc for 24 h. Firefly luciferase (*Luc*) activity was normalized to *Renilla* luciferase as a transfection efficiency control. The level of activity of the promoterless *Renilla* plasmid luciferase was defined as 1. The results depicted are the averages of three independent experiments; *error bars* indicate S.D. # indicates mutation of CHR, and ** indicates mutation of CDE. *B*, nucleotide sequences of the human *survivin* promoter and three mutants. *Underlines* indicate CHR or CDE region. *Shaded characters* indicate mutation (*mut*). *C*, EMSA. Nuclear lysates extracted from Nalm-6/E2A-HLF cells cultured without (*lanes 1* and *3–5*) or with zinc (*lane 2*) were incubated with a ^{32}P-end-labeled oligonucleotide probe containing the CHR sequence (*lanes 1–4*) or mutated CHR sequence (*lane 5*). An excess of unlabeled CHR sequence competitor (*lane 3*) or mutant competitor (*lane 4*) was added to the reaction mixture. *Mt*, mutant.

surement of externalized phosphatidylserine with the annexin-V-FITC apoptosis detection kit I (BD Biosciences) in preparation for flow cytometry with the FACScan/CellFIT system (BD Biosciences). For caspase inhibition, 20 μM benzyloxycarbonyl-VAD-fluoromethyl ketone (BD Biosciences) was added to the cells 1 h before the addition of zinc. Terminal deoxynucleotidyltransferase-mediated dUTP nick-end-labeling (TUNEL) was performed using the apo-BrdUrd TUNEL assay kit (Molecular Probes, Eugene, OR). Briefly, cells fixed with paraformaldehyde and ethanol were incubated with BrdUrd and TdT for 1 h at 37 °C. BrdUrd uptakes were detected by Alexa dye-leveled anti-BrdUrd antibodies. Cells were stained by PI just before analysis using FACScan/CellFIT system.

RESULTS

E2A-HLF Regulates Survivin Expression—Cell lines were used in this study instead of primary patient samples, because t(17;19)$^+$ ALLs constitute only ~1% of childhood B-precursor ALLs (1–3). Four t(17;19)$^+$ ALL cell lines (UOC-B1, YCUB-2, HAL-O1, and Endo-kun) expressed the E2A-HLF chimeric protein on immunoblot analysis (Fig. 1*A*, *4th panel, lanes 1–4*) either as a slower (*lanes 1* and *3*) or a faster migration band (*lanes 2* and *4*) corresponding to difference in the fusion junction, as described previously (3). Of the seven t(17;19)$^-$ leukemia cell lines tested (RS4;11, Nalm-6, REH, 920, Jurkat, HL-60 and NB-4), none expressed the E2A-HLF chimera (Fig. 1*A*, *lanes 5–11*). We performed Northern blot and immunoblot analyses to test human leukemia cell lines for the expression of *survivin*. Survivin mRNA and protein were expressed at uniformly high levels in the four t(17;19)$^+$ ALL cell lines (Fig. 1*A*, *top* and *3rd panels*). By contrast, *survivin* mRNA levels varied among the t(17;19)$^-$ leukemia cell lines and appeared to determine Survivin protein expression levels in each line (Fig. 1*A*, *lanes 5–11*).

Next, we tested whether E2A-HLF induces the expression of Survivin. For these experiments, Nalm-6 cells were transfected with a pMT-CB6+/E2A-HLF construct to generate clones (Nalm-6/E2A-HLF) with zinc-inducible expression of E2A-HLF (Fig. 1*B*, *4th panel*). Ectopic expression of E2A-HLF in Nalm-6 cells induced *survivin* mRNA by 5-fold within 24 h after the addition of zinc (Fig. 1*B*, *top panel*). Accordingly, Survivin protein expression increased within 24 h after induction of E2A-HLF (Fig. 1*B*, *3rd panel*). In control Nalm-6/pMT cells, which contained the empty vector, Survivin expression was unaffected by zinc (Fig. 1*B*, *lanes 7* and *8*), confirming that the observed changes in Survivin expression were induced by E2A-HLF and not by zinc.

Induction of Survivin by E2A-HLF was further confirmed using UOC-B1/E2A-HLF(dn) cells, which express zinc-inducible E2A-HLF(dn), a dominant negative mutant of E2A-HLF (see under "Experimental Procedures") (6, 19). Survivin mRNA and protein expression in UOC-B1/E2A-HLF(dn) cells were high in the absence of zinc (Fig. 1*C*, *top* and *3rd panels, lane 1*; see also Fig. 1*D*) but decreased within 24 h after the addition of

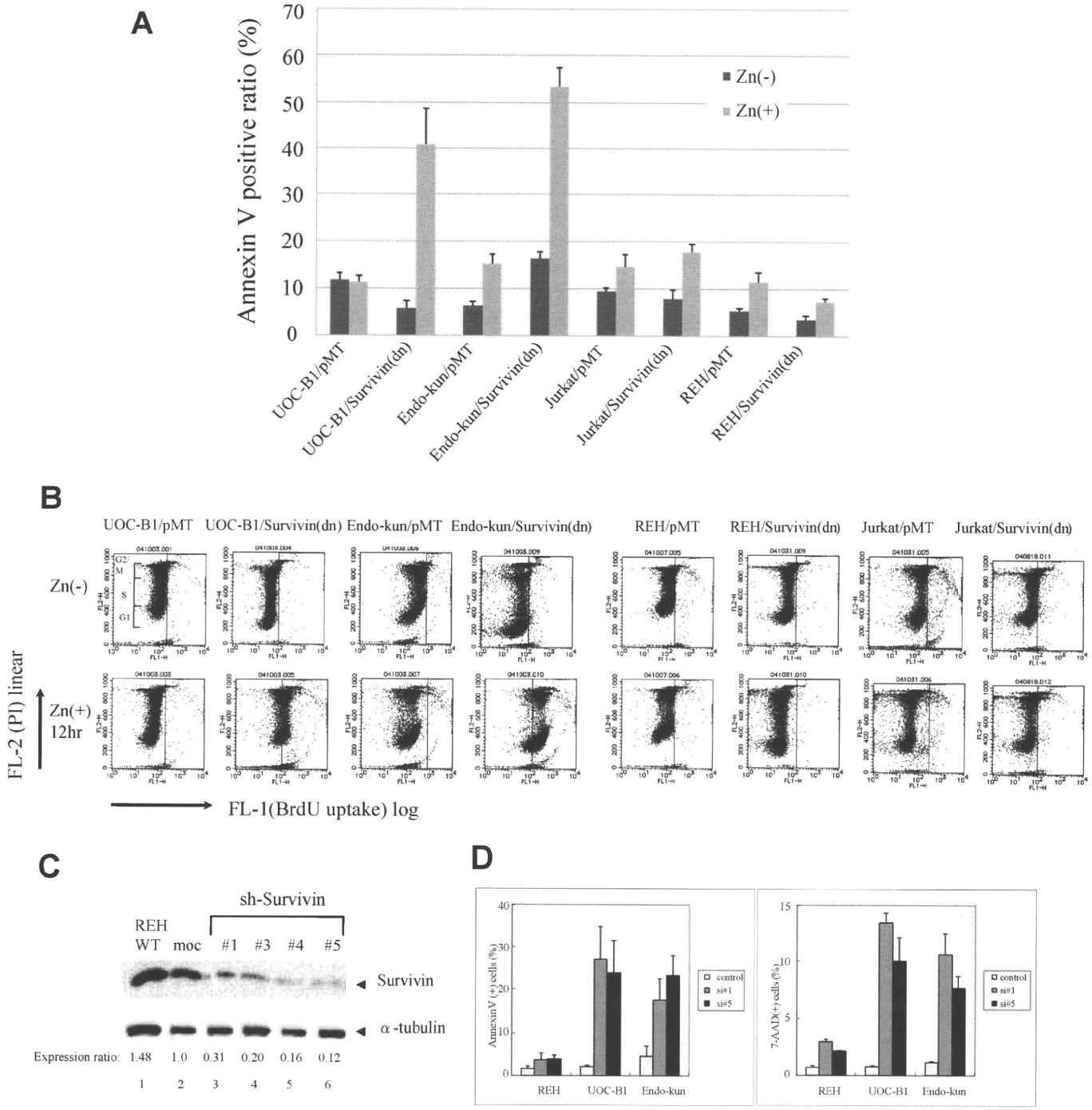

FIGURE 4. **Effect of enforced overexpression of Survivin-T34A and introduction of Survivin-shRNA in ALL cells.** UOC-B1, Endo-kun, Jurkat, and REH cells inducibly expressing Survivin-T34A (UOC-B1/Survivin(dn), Endo-kun/Survivin(dn), Jurkat/Survivin(dn) and REH/Survivin(dn) cells, respectively) were compared with control UOC-B1/pMT, Endo-kun/pMT, Jurkat/pMT, and REH/pMT cells, respectively. *A*, externalization of phosphatidylserine as determined by annexin-V binding. Cells cultured in medium with or without 100 μM zinc for 24 h were simultaneously stained with FITC-annexin-V and PI. The FITC-annexin-V-positive ratios were determined by representative flow cytometric plots. *B*, cells cultured in medium with or without 100 μM zinc for 12 h were simultaneously stained with PI and BrdUTP in a TdT-catalyzed reaction and then subjected to flow cytometric analysis. DNA ends labeled with BrdUTP (*abscissa*) are shown as a function of cellular DNA content of PI-stained nuclei (*ordinate*). Cells to the *right* of the *vertical line* had free DNA ends labeled with TdT, indicating apoptosis. Range of each cell cycle was shown in the panel of UOC-B1/pMT, *Zn*(−). *C*, immunoblot analyses using Survivin (*upper panel*) and α-tubulin (*lower panel*) antibodies. REH cells without treatment (*lane 1*) or infected with lentivirus (*lanes 2–6*) were sorted by GFP expression. *moc* indicates control sh-RNA. Ratios of intensity are shown *below*. *WT*, wild type. *D*, ratios of annexin-V-phycoerythrin (*PE*) (*left*) or 7-AAD (*right*)-positive cells in the GFP-positive fraction of REH, UOC-B1, or Endo-kun cells infected with lentivirus expressing GFP alone (control) or GFP and Survivin shRNA1 or -5 (*si#1* or *si#5*, respectively). Mean values from three independent experiments are shown with standard error.

zinc (Fig. 1*C*, *lane 5*), coincident with expression of E2A-HLF(dn) protein (*4th panel*). Removal of zinc from the growth medium restored Survivin expression within 48 h, again coincident with a decline in the E2A-HLF(dn) protein level (Fig. 1*C*, *lane 9*). These data suggested that E2A-HLF induces Survivin mRNA expression. Down-regulation of Survivin protein pre-

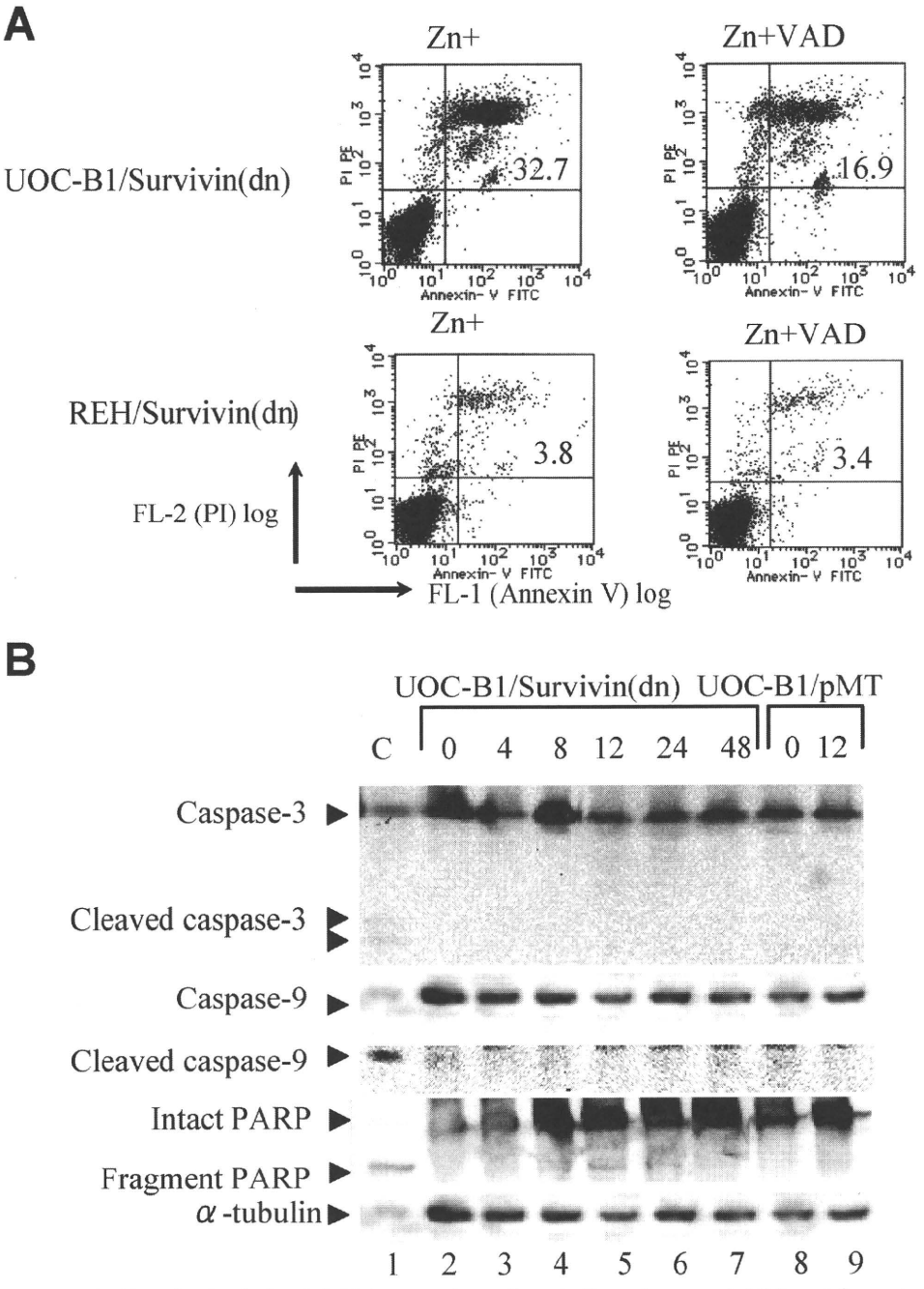

FIGURE 5. **PARP activation in Survivin(dn)-expressing cells and effect of caspase inhibitor.** *A*, flow cytometric analysis stained with annexin-V (*abscissa*) and PI (*ordinate*). UOC-B1/Survivin(dn) and REH/Survivin(dn) cells were cultured in medium containing 100 μM zinc 1 h after treatment with or without 20 μM benzyloxycarbonyl-VAD-fluoromethyl ketone (*VAD*), a pan-caspase inhibitor. *B*, UOC-B1/Survivin(dn) or UOC-B1/pMT cells were cultured in medium containing 100 μM zinc for the indicated times. Immunoblot analysis of UOC-B1/Survivin(dn) cells was performed to detect caspase-3, cleaved caspase-3, caspase-9, cleaved caspase-9, intact PARP, fragmented PARP, and α-tubulin proteins. As a positive control (*C*), Jurkat cells were treated with etoposide.

ceded the reduction of Survivin mRNA (Fig. 1*D*), suggesting the involvement of post-transcriptional mechanism(s).

Cell Cycle-independent Induction of Survivin by E2A-HLF—The Survivin mRNA and protein levels at the G_2/M phase of the cell cycle are more than 10-fold higher than those at the G_1 phase in NIH3T3 murine fibroblasts synchronized by serum starvation and in drug-synchronized HeLa cells (17, 25). Because it is difficult to synchronize leukemia cells by serum starvation or by reagents inhibiting cell cycle progression at a specific phase, we performed counterflow centrifugal elutriation to enrich cells at each phase of the cell cycle. The purity of the preparations was typically more than 90% for G_0/G_1-phase cells, more than 80% for S-phase cells, and ~90% for G_2/M-phase cells (Fig. 2*A*). We performed immunoblot analysis to measure Survivin expression in the enriched fractions. In t(17;19)$^-$ ALL cell lines (RS4;11, REH, and 920), Survivin expression was most evident at the G_2/M-phase (Fig. 2, *B, lanes 13–21,* and *C*). In particular, 920 cells at the G_2/M phase showed ~11- and 4-fold higher expression than those at the G_1 and S phase, respectively. By contrast, the four cell lines harboring the E2A-HLF chimeric protein expressed Survivin at high levels throughout the cell cycle (Fig. 2, *B, lanes 1–12,* and *C*).

E2A-HLF Enhances the Promoter Activity of the Survivin Gene—To elucidate how E2A-HLF induces expression of the *survivin* gene, we analyzed the effects of E2A-HLF on the function of the *survivin* promoter. We initially generated reporter plasmid vectors (pGL3-124, -190, -265, -480, and -675), each of which contained a different length of human *survivin* promoter. These vectors were analyzed for luciferase activity in transiently transfected Nalm-6/E2A-HLF cells. When cells were cultured without zinc, luciferase activity was low in cells transfected with pGL3-124 (Fig. 3*A*). Transfection of pGL3-190 resulted in the highest luciferase activity; it was nearly 6-fold higher than that which resulted from transfection of pGL3-124. However, transfection of *survivin* constructs longer than pGL3-265 resulted in significantly less activity compared with that of pGL3-190, suggesting the presence of enhancer elements in the region from nt −124 to −190 and repressor elements in the region upstream of nt −190. When cells were cultured with zinc for 24 h, the luciferase activity of each reporter construct, including the shortest pGL3-124, increased by ~3-fold compared with the respective cells cultured without zinc, suggesting that E2A-HLF induces *survivin* transcription through *cis* elements in the region from nt 0 to −124.

To further investigate the mechanism through which E2A-HLF induces transcription of the *survivin* gene, we used luciferase reporter constructs with mutated cell cycle-dependent *cis* elements. These elements, including the cell cycle-dependent element (CDE; GGCGG) and the cell cycle homology region (CHR; ATTTGAA), are implicated in G_1 transcriptional repression in S/G_2-regulated genes, such as cyclin A, cdc25C, and cdc2 (18). A previously published report demonstrated two CDEs (−6 and −12) and one CHR (−42) in the human *survivin* promoter between nt 0 and −124 (Fig. 3*B*) (18). When pGL3-124mut1, which contained mutated CDE-6 and CDE-12 but had intact CHR-42, was transfected in Nalm-6/E2A-HLF cells, the level of luciferase activity was virtually the same as that of pGL3-124 regardless of the presence of zinc, suggesting that CDE-6 and CDE-12 do not contribute to regulation of *survivin* transcription in Nalm-6 cells (Fig. 3*A*). By contrast, transfection of pGL3-124mut2, which contained mutated CHR-42 in addition to mutated CDE-6 and CDE-12, resulted in 10-fold higher luciferase activity in the absence of zinc and 3-fold higher luciferase activity in the presence of zinc compared with transfection of pGL3-124. As a result, there was virtually no difference in the level of luciferase activity between the presence or absence of zinc in cells transfected with pGL3-124mut2. Transfection of pGL3-124mut3, in which only CHR-42 was mutated, show similar results as transfection of pGL3-124mut2. These results suggested that E2A-HLF directly or indirectly up-regulates transcription of *survivin* through a CHR-42 silencer.

To elucidate transcription factors that bind to CHR-42, we performed EMSA. Smear-looking CHR probe-protein complexes were readily detected (Fig. 3*C*, *lane 1*) and were ablated by the addition of an excess amount of cold competitor (*lane 3*) but not by mutated CHR competitor (*lane 4*). These complexes were not detected when using mutated CHR as a probe (Fig. 3*C*, *lane 5*), suggesting that this complex represents specific binding between transcription factor(s) and the CHR sequence. When E2A-HLF was induced by the addition of zinc, the intensity of the smear decreased (Fig. 3*C*, *lane 2*), further supporting that E2A-HLF up-regulates expression of *survivin* via a CHR-42 silencer.

Specific Inhibition of Survivin-induced Apoptosis in t(17;19)$^+$ ALL Cell Lines—To test whether induction of Survivin by E2A-HLF is essential for the survival of t(17;19)$^+$ leukemia cells, we initially used zinc-inducible expression of a phosphorylation-defective Survivin mutant (Survivin-T34A) that functions as a dominant negative inhibitor. An annexin-V binding assay was used to measure externalization of phosphatidylserine, an indicator of cell death. Ectopic expression of Survivin-T34A in two t(17;19)$^+$ ALL cell lines (UOC-B1 and Endo-kun) caused a rapid increase in the fraction of annexin-V-positive cells within 24 h after the addition of zinc (Fig. 4*A*). In control UOC-B1/pMT and Endo-kun/pMT cells, which contained the empty vector, less than 20% of cells were positive for annexin-V regardless of the presence of zinc. By contrast, Survivin-T34A did not induce massive cell death in two t(17;19)$^-$ leukemia cell lines (REH and Jurkat), which express relatively high levels of Survivin (Fig. 1*A*). The basis for the altered survival of UOC-B1 and Endo-kun cells expressing Survivin-T34A was investigated by TUNEL analysis using flow cytometry. BrdUrd uptake (Fig. 4*B*, *x* axis) by TdT that reflects a number of DNA ends in each cell was markedly increased in UOC-B1 and Endo-kun cells expressing Survivin-T34A. Interestingly, intensities of BrdUrd signals increased equally in cells at each cell cycle phase (*y* axis), suggesting that down-regulation of Survivin function induces apoptosis in a cell cycle-independent manner. By contrast, expression of Survivin-T34A did not induce apoptosis in REH cells and induced apoptosis in Jurkat cells only at the G_2/M phase (Fig. 4*B*).

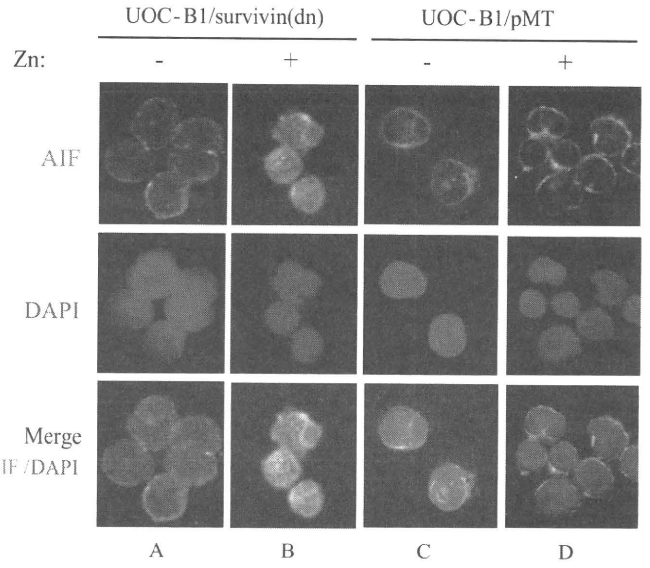

FIGURE 6. **Effect of Survivin(dn) on nuclear translocation of AIF.** UOC-B1/Survivin(dn) cells (*A* and *B*) or UOC-B1/pMT cells (*C* and *D*) were cultured for 12 h in the absence of zinc (*A* and *C*) or in the presence of 100 μM zinc (*B* and *D*). Cells were immunostained with an anti-AIF polyclonal antibody (*upper panels*). Cells were stained with 4′,6-diamidino-2-phenylindole (*DAPI*) to visualize the nuclei (*middle* and *lower panels*).

We next down-regulated Survivin by lentivirally introduced short hairpin (sh) RNA. The Survivin protein expression level in cells sorted by expression of GFP (as an indicator of infection) was significantly reduced by Survivin-shRNA1 and -3–5 compared with that in cells infected with control-shRNA (Fig. 4*C*). We introduced shRNA1 or -5 into REH, UOC-B1, and Endo-kun cells. Twenty four hours later, when about 10% of the cells were GFP-positive, dead cells were determined by annexin-V and 7-AAD staining. Marked increases in annexin-V- and 7-AAD-positive cells were detected in the GFP-positive population of UOC-B1 or Endo-kun cells compared with those in GFP-positive REH cells (Fig. 4*D*).

Caspase-dependent and -independent Cell Death Are Induced by Survivin-T34A in t(17;19)$^+$ Cells—To elucidate the molecular mechanisms through which Survivin protects t(17;19)$^+$ ALL cells from apoptosis, we initially examined caspase-dependent pathways. A pan-caspase inhibitor, benzyloxycarbonyl-VAD-fluoromethyl ketone, partially blocked cell death induced by Survivin-T34A (Fig. 5*A*). Immunoblot analysis revealed fragmentation of PARP within 8 h after induction of Survivin-T34A, although cleavage of caspase-3 and -9 was barely detectable up through 48 h (Fig. 5*B*). These results suggested that caspase-independent pathways contribute to cell death induced by Survivin-T34A in t(17;19)$^+$ ALL cells.

The association of Survivin targeting both preceding and independent of caspase activation suggested to us a potential role for AIF, given its capacity to mediate DNA fragmentation

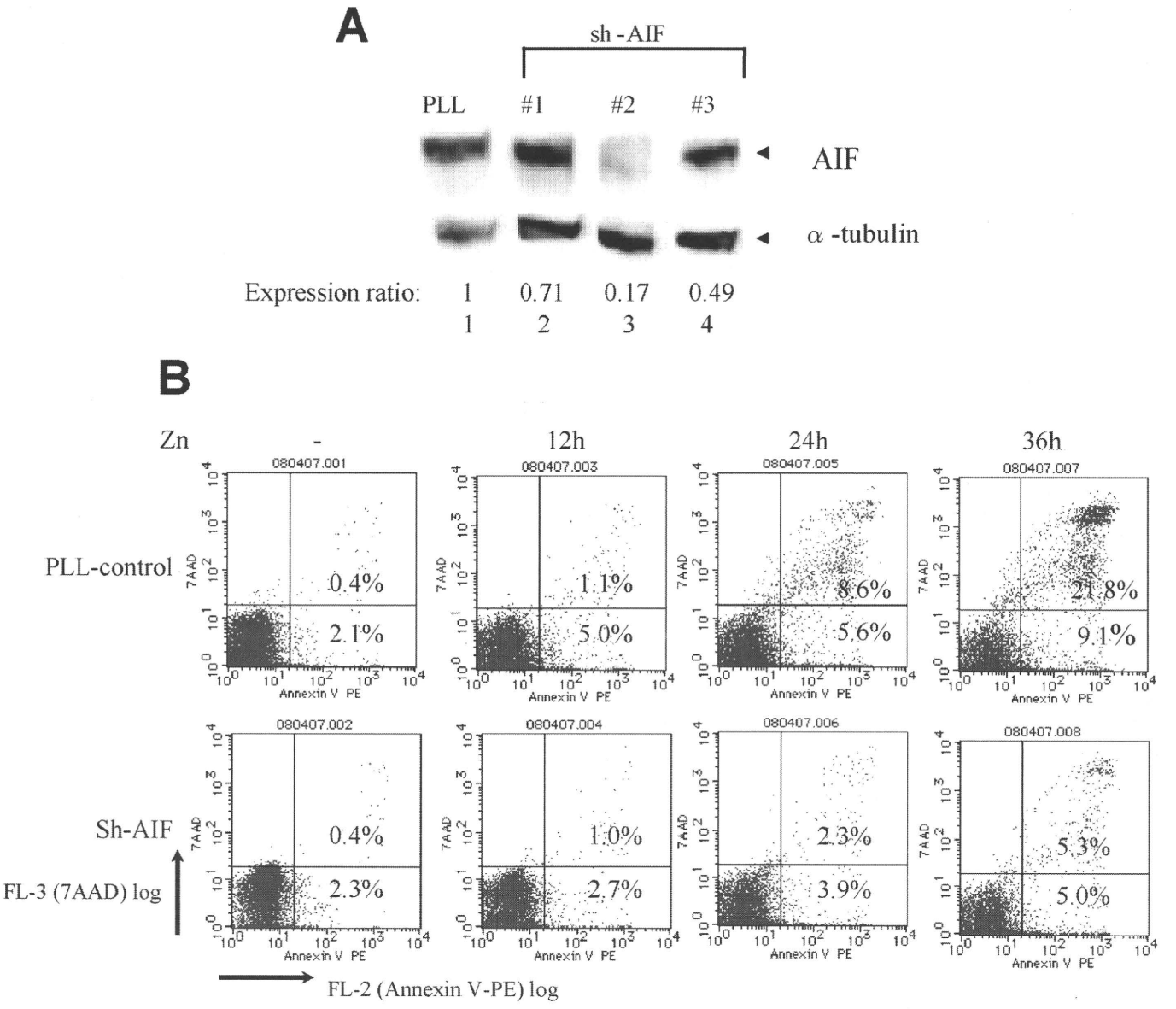

FIGURE 7. **Inhibition of Survivin-T34A-induced apoptosis by knockdown of AIF.** *A,* immunoblot analysis using AIF (*upper panel*) or α-tubulin (*lower panel*) antibodies. UOC-B1/Survivin(dn) cells were infected with lentivirus expressing the shRNA indicated *above* each panel, and GFP-positive cells were sorted. Ratios of intensity are shown *below*. *B,* UOC-B1/Survivin(dn) cells were infected with lentivirus expressing control-shRNA (*PLL, upper*) or AIF-shRNA2 (*lower*), cultured with 100 μM zinc for the indicated length of time, and stained with annexin-V-phycoerythrin (*PE*) (*abscissa*) and 7-AAD (*ordinate*). The data show the ratio of annexin-V-phycoerythrin- and 7-AAD-positive cells in the GFP-positive fraction as determined by flow cytometric analysis. *Numbers* indicate the percentage of apoptotic cells.

and cytochrome *c* release in a caspase-independent fashion (28, 29). We analyzed the nuclear translocation of AIF after induction of Survivin-T34A in t(17;19)$^+$ ALL cells. In the UOC-B1/Survivin(dn) cells without induction of Survivin-T34A, AIF signals were found in the cytoplasm in ~75% of the total cell population (Fig. 6*A*), consistent with a previous report showing the presence of AIF in mitochondria (27). By contrast, expression of Survivin-T34A for 12 h induced nuclear translocation of AIF signals in more than 90% of cells (Fig. 6*B*). Nuclear translocation of AIF was induced in only a small percentage (~ 4%) of the control UOC-B1/pMT cells treated with zinc (Fig. 6*D*).

To test the role of AIF in cell death induced by Survivin-T34A in t(17;19)$^+$ ALL cells, we down-regulated AIF expression by lentivirally expressed AIF-shRNA. The AIF protein expression level in UOC-B1/Survivin(dn) cells was significantly reduced by AIF-shRNA2 compared with that in cells infected with control PLL-shRNA sorted by expression of GFP (Fig. 7*A*). The number of cells undergoing cell death by induction of Survivin-T34A was monitored by annexin-V and 7-AAD staining in GFP-positive cells. Cells treated with AIF-shRNA2 were significantly resistant to cell death compared with those treated with control PLL-shRNA (Fig. 7*B*), suggesting that AIF plays critical roles in Survivin-mediated cell death of t(17;19)$^+$ ALL cells.

DISCUSSION

We previously demonstrated that E2A-HLF contributes to leukemogenesis of t(17;19)-positive ALL through inhibition of apoptosis (6). Here, we demonstrate that E2A-HLF induces Survivin expression through transcriptional regulation. Down-

regulation of Survivin function by a dominant negative mutant of Survivin (Survivin-T34A) or reduction of Survivin expression by shRNA induced massive apoptosis in t(17;19)$^+$ leukemia cells throughout the cell cycle. Down-regulation of Survivin induced apoptosis via both caspase-dependent and -independent pathways, and AIF was involved in the latter pathways. These findings indicate that Survivin plays critical roles in E2A-HLF-mediated leukemogenesis.

E2A-HLF, known as a *trans*-activator (24), could either directly or indirectly enhance *survivin* transcription. However, there is no potential binding site of E2A-HLF (GTTACGTAAT) in the promoter region of *survivin*, and indeed, no binding activity of E2A-HLF was detected by EMSA in the immediate upstream region (124 bp) of the initial ATG, including a region that contains CHR-42 sequence (ATTTGAA) (negative data not shown). Thus, E2A-HLF most likely inhibits the silencer activity of CHR-42 (Fig. 3*A*) by down-regulating a certain amount of hypothetical *trans*-repressor *X* that binds to CHR-42 (Fig. 3*C*, *lane 2*). Theoretically, E2A-HLF may induce another *trans*-repressor that down-regulates the expression of *trans*-repressor *X*. Alternatively, a downstream target factor of E2A-HLF may reduce the DNA binding potential of *trans*-repressor *X*. It is of interest to note that whether or not the mechanism through which E2A-HLF induces *survivin* transcription is common to that, Ras pathways regulate Survivin expression. As we reported previously (30), because downstream targets of Ras enhance Survivin expression through enhancer(s) between −124 to −190, E2A-HLF likely induces Survivin through distinctive pathways.

Previous reports indicated that Survivin inhibits apoptosis through both caspase-dependent and caspase-independent pathways, although detailed mechanisms are not yet understood (31–34). In t(17;19)$^+$ ALL cells undergoing apoptosis by Survivin-T34A, activation of the caspase cascade is likely a secondary event, because activated caspase-3 and -9 were not detectable up through 48 h after induction of Survivin-T34A (Fig. 5*B*), even though the cells were positive on annexin-V staining and TUNEL analysis within 12 h (Fig. 4, *A* and *B*). We observed rapid PARP activation within 8 h that is required for translocation of AIF to the nucleus from mitochondria, followed by morphological changes such as cell shrinkage and chromatin condensation (27, 35). Moreover, knockdown of AIF in UOC-B1/Survivin(dn) cells protected cells from apoptosis induced by Survivin-T34A (Fig. 7*B*). Therefore, reversal of AIF translocation by Survivin, which is induced by E2A-HLF throughout the cell cycle, appears to be the key mechanism in the protection of t(17;19)$^+$ leukemia cells from apoptosis.

In earlier studies, we identified *SLUG* as a target gene of E2A-HLF (36). SLUG is a transcription factor closely related to Ces-1, a cell death regulator in *Caenorhabditis elegans* (36, 37). Importantly, *ces-1* is a downstream target gene of *ces-2*, which is closely related to E2A-HLF (6, 38). The apparent convergence of cell death pathways, including CES-2/CES-1 in the worm and E2A-HLF/SLUG in human pro-B leukemia (6, 36), suggests that SLUG may have an important regulatory role in the survival of lymphoid cells. However, the lack of expression of Slug by normal pro-B cells suggests that E2A-HLF acts not by invoking a normal survival pathway in B lymphocytes but rather by aberrantly activating a Slug-mediated survival pathway normally used by more primitive hematopoietic cell progenitors (39). Therefore, it is still uncertain whether only the E2A-HLF/SLUG pathway inhibits apoptosis in leukemia pro-B cell progenitors (36). Perhaps E2A-HLF has multiple apoptosis-inhibiting pathways to coordinate leukemogenesis.

t(17;19)$^+$ ALL almost always proves refractory to intensive chemotherapy, even to the aggressive conditioning for bone marrow transplantation (3–5). Survivin is an attractive therapeutic target in t(17;19)$^+$ ALLs because of its differential expression in tumors *versus* normal tissues and because it may be required for maintaining cell viability in this leukemia (14, 16). The efficacy of Survivin antisense oligonucleotides has been demonstrated *in vivo* (40, 41), and clinical grade antisense Survivin oligonucleotides are currently under development (42, 43). Although Survivin is not a cancer-specific molecule in regulating normal cell function particularly in the hematopoietic stem cell and immune systems, anti-Survivin therapies developed to date have not revealed major systemic toxicities in animal models and are encouraging (44). Our results provide further evidence that Survivin inhibitors may be an effective therapeutic strategy for this refractory ALL.

Acknowledgments—We thank M. Eguchi for helpful discussions, support, and encouragement throughout this study and Y. Sato for support and encouragement. We thank F. J. Rauscher III for providing the pMT-CB6$^+$ expression vector; K. Harada, H. Aoyama, and M. Ishiguchi for excellent technical assistance; K. Ohyashiki and K. Toyama for HAL-O1 cell lines; and M. Endo for Endo-kun cell lines.

REFERENCES

1. Inaba, T., Roberts, W. M., Shapiro, L. H., Jolly, K. W., Raimondi, S. C., Smith, S. D., and Look, A. T. (1992) *Science* **257,** 531–534
2. Hunger, S. P., Ohyashiki, K., Toyama, K., and Cleary, M. L. (1992) *Genes Dev.* **6,** 1608–1620
3. Hunger, S. P. (1996) *Blood* **87,** 1211–1224
4. Inukai, T., Hirose, K., Inaba, T., Kurosawa, H., Hama, A., Inada, H., Chin, M., Nagatoshi, Y., Ohtsuka, Y., Oda, M., Goto, H., Endo, M., Morimoto, A., Imaizumi, M., Kawamura, N., Miyajima, Y., Ohtake, M., Miyaji, R., Saito, M., Tawas, A., Yanai, F., Goi, K., Nakazawa, S., and Sugita, K. (2007) *Leukemia* **21,** 288–296
5. Matsunaga, T., Inaba, T., Matsui, H., Okuya, M., Miyajima, A., Inukai, T., Funabiki, T., Endo, M., Look, A. T., and Kurosawa, H. (2004) *Blood* **103,** 3185–3191
6. Inaba, T., Inukai, T., Yoshihara, T., Seyshab, H., Ashmun, R. A., Canman, C. E., Laken, S. J., Kastan, M. B., and Look, A. T. (1996) *Nature* **382,** 541–544
7. Inukai, T., Inaba, T., Okushima, S., and Look, A. T. (1998) *Mol. Cell. Biol.* **18,** 6035–6043
8. Kinoshita, T., Yokota, T., Arai, K., and Miyajima, A. (1995) *EMBO J.* **14,** 266–275
9. Kuribara, R., Kinoshita, T., Miyajima, A., Shinjyo, T., Yoshihara, T., Inukai, T., Ozawa, K., Look, A. T., and Inaba, T. (1999) *Mol. Cell. Biol.* **19,** 2754–2762
10. Ikushima, S., Inukai, T., Inaba, T., Nimer, S. D., Cleveland, J. L., and Look, A. T. (1997) *Proc. Natl. Acad. Sci. U.S.A.* **94,** 2609–2614
11. Ambrosini, G., Adida, C., and Altieri, D. C. (1997) *Nat. Med.* **3,** 917–921
12. Sommer, K. W., Stumberger, C. J., Schmidt, G. E., Sasgary, S., and Cerni, C. (2003) *Oncogene* **22,** 4266–4280
13. Tamm, I., Wang, Y., Sausville, E., Scudiero, D. A., Vigne, N., Oltersdorf, T., and Reed, J. C. (1998) *Cancer Res.* **58,** 5315–5320
14. Li, F. (2003) *J. Cell. Physiol.* **197,** 8–29